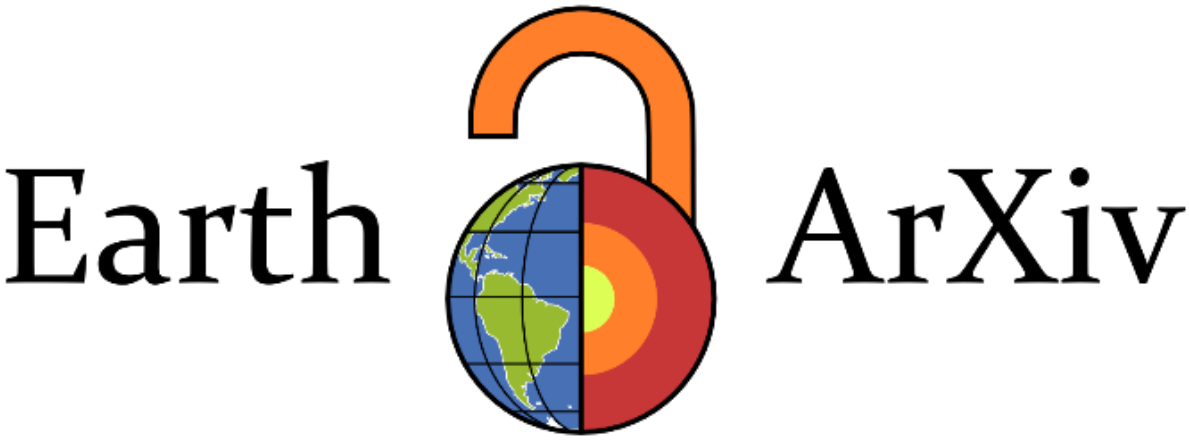

Graphical Abstract

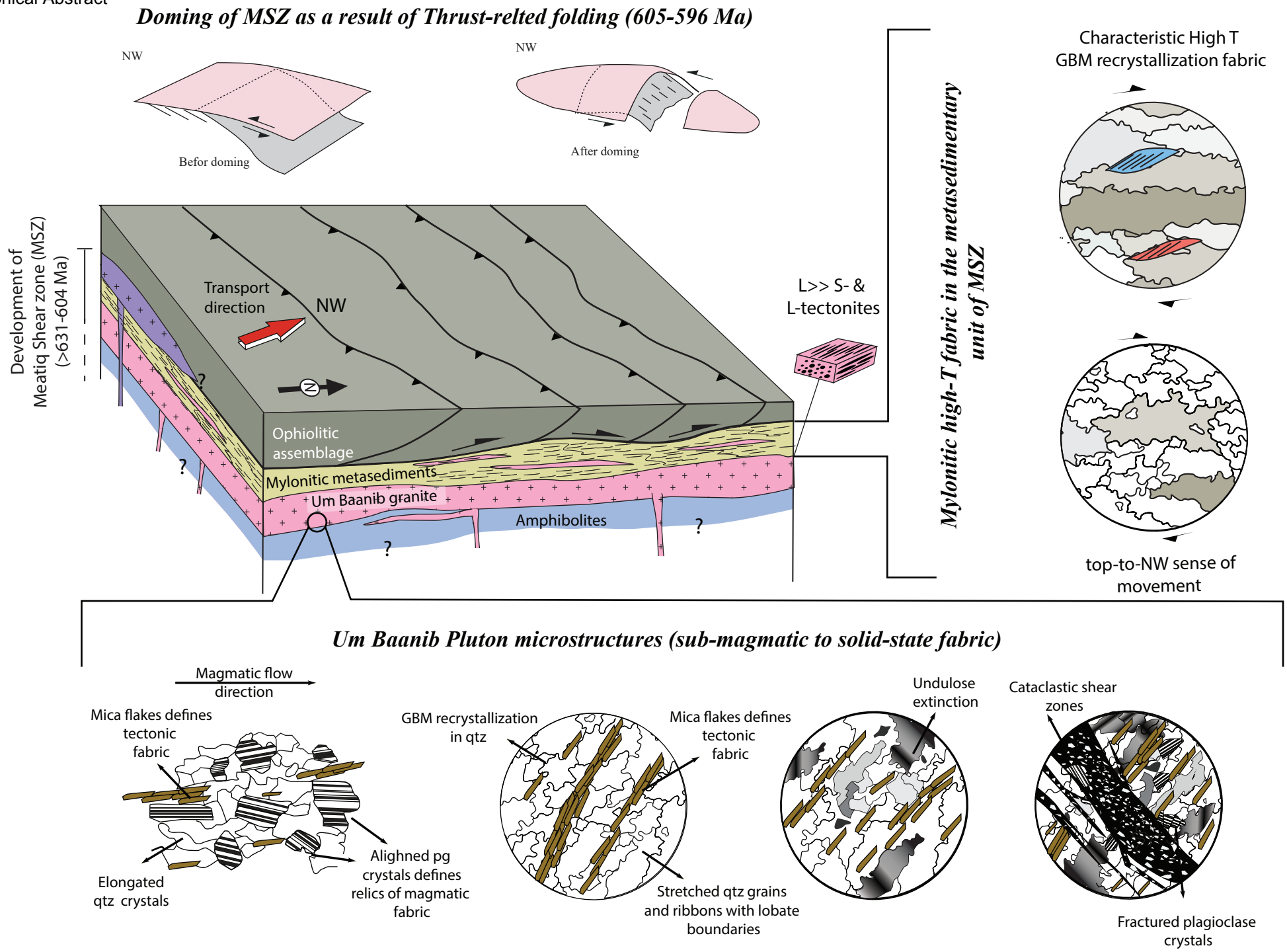

Rethinking the Anatomy and Architecture of the Neoproterozoic Gneiss Domes in the Nubian Shield: Are they Extensional Metamorphic Core Complexes?

Abdullah. T. Mohammad[1, 2], Yahia. A. El Kazzaz[2]

[1] Department of Geological and Environmental Sciences, Western Michigan University, Kalamazoo, MI 49008, USA
[2] Department of Geology, Helwan University, 11795 Helwan, Cairo, Egypt

Abstract

The Nubian Shield features amphibolite-grade, gneiss-cored domes surrounded by greenschist-grade island arc and ophiolitic assemblages. These structures exhibit anomalous intense ductile deformation and higher metamorphism than the surrounding rock units; yet, their nature, geometry, and origin remain controversial. The present study integrates field data, remote sensing, and detailed structural and microstructural analyses to reevaluate the nature, architecture, and formation of these metamorphic domes, focusing on the Meatiq dome in Egypt's Central Eastern Desert. Our findings reveal: (1) Meatiq Dome comprises a domed thrust shear zone originating at mid-crustal depths, initially oriented sub-horizontally. Microstructural analysis shows the dominance of crystal plastic deformation with non-coaxial strain and varying metamorphic conditions. (2) The granite plutons in the dome (Um Baanib and Abu Ziran) were emplaced syn-kinematically during NW-ward tectonic transport, strongly supported by the sub-magmatic microstructures that reflect concurrent magmatic and solid-state deformation. Both plutons exhibit sheet-like geometries and were emplaced along distinct rheological contacts. (3) While the Meatiq Dome shares some attributes with metamorphic core complexes (MCCs), such as low-angle shear surfaces and mylonitic rocks, it lacks typical MCC features like low-angle and rotational normal faults. Structural analysis indicates that the domiform geometry of these structures is better explained by thrust-related folding rather than by MCC models. The deformation history of the Meatiq Dome comprises five key phases related to different tectonic stages with ages ranging from Precambrian to Cenozoic. The results provide new insights into the 3D geometry and structural history of the gneiss domes in the Nubian Shield, with implications for deformation processes in mid-crustal shear zones.

1. Introduction

The East African Orogen is a major mobile belt formed through prolonged accretion and collisions, culminating in the collision of East and West Gondwanaland around 600 Ma (Stern 1994; Meert 2003; Johnson et al., 2011). The orogen comprises the southern Mozambique Belt, characterized by intense deformation and high-grade metamorphism, and reworked crustal remnants; and the northern Arabian-Nubian Shield (ANS), a juvenile belt with lower deformation and metamorphic grades (Abdelsalam and Stern, 1996). However, the ANS hosts several domiform metamorphic complexes (e.g., Meatiq, Hafafit, Feiran-Solaf) with intense deformation and medium- to high-grade metamorphism (Fritz et al., 1996; Greiling, 1997; Fowler et al., 2007; Andresen et al., 2010; Fowler and Hamimi 2020). These intriguing structures comprise complex suites of amphibolite-facies metasediments, metavolcanics, amphibolites, and deformed plutonic rocks, and are detached from overlying ophiolitic nappes and tectonic mélanges by a mylonitic carapace (Sturchio et al., 1983; Fritz et al., 1996; Andresen et al., 2010). Despite extensive research, the mechanisms driving the evolution of these complexes remain unclear.

The earlier models were inspired by the gneiss domes model of Eskola (1949). In this sense, ANS's metamorphic complexes were defined as mantled gneiss domes developed through two subsequent orogenic episodes (Schürmann 1966; Habib et al., 1985a, b). The recognition of similarities between these domes and the Cordilleran MCCs in terms of structural architecture and metamorphic conditions (Sturchio et al., 1983) prompted a reevaluation of these structures as MCCs formed in an extensional regime (Fritz et al., 1996; Blasband et al., 2000). Meanwhile, it has been widely noted that gneiss domes in the Arabian Shield are spatially coupled with a network of NW- trending transcurrent shear zones known as the Najd Shear System (NSS, e.g., Agar, 1987; Hamimi and Fowler., 2021). Identifying NSS extensions in the Nubian Shield (e.g., Sultan et al., 1988) paved the way for models linking gneiss domes evolution to NSS activity (e.g., Fritz et al., 1996, 2002; Hassan et al., 2016; Makroum, 2017).

Fritz et al. (1996) proposed that the gneiss domes in the Central Eastern Desert (CED) are extensional MCCs aligned along NW-trending brittle-ductile shear zones, referred to as wrench corridors, and the exhumation of these core complexes was controlled by orogen parallel extension accommodated by strain partitioning in these corridors. This model underwent extensive deliberation during the 2000s and incorporated other mechanisms such as exhumation in transtensional jogs and stepovers (e.g., Meyer et al., 2014), transpressional scissor-shaped corridors (Shalaby, 2010), and megascale flower structures (Makroum, 2017). Over the last two decades, this paradigm has been central to understanding the ANS's structural evolution. Nonetheless, the accumulation of structural data contradicting this model, triggered a growing body of robust refutation. The points of contention can be identified in these debates: (1) the presence of extensions for the NSS in the Nubian Shield (e.g., El Ramly et al., 1990), (2) tectonic setting for the evolution of the domes (extensional vs. shortening; Greiling 1997; Greiling et al., 1994; Andresen et al., 2010), (3) geometry and origin of shear zones in the CED which is the most contentious aspect of the ongoing debate (e.g., Fowler and El Kalioubi 2004; Andresen et al., 2010; Mohammad et al., 2020), (4) nature and geometry of the metamorphic domes (Fowler and Osman 2001; Fowler and El Kalioubi 2002; Fowler et al.,2018), and (5) the temporal relationships among

deformation, metamorphism, and magmatism episodes (e.g., Abu Sharib et al., 2019; El Kalioubi et al., 2020).

The Meatiq Dome, located in CED, is a key area for addressing these issues. It is an elliptical dome structure, measuring 22 km by 18 km. Its western boundary is marked by the NW-SE trending Atalla Shear Zone (ASZ), a crustal-scale transpressional zone with sinistral shear (Mohammad et al., 2020). While most studies have focused on the regional structural framework, the internal anatomy of the lithological units and igneous plutons within the dome has received limited attention. Additionally, most studies emphasize Neoproterozoic deformation phases, with little focus on Phanerozoic phases. This work aims to reappraise the 3D geometry of the Meatiq dome, investigate the Meatiq shear zone's (MSZ) genesis, and develop a comprehensive model for its spatial and temporal evolution. The study compiles data from remote sensing, geological mapping, and structural and microstructural analysis. The findings provide new insights into the 3D geometry and history of "gneiss domes" in the ANS, test and validate their classification as MCCs. In addition, results offer valuable implications for understanding the structural, magmatic, and tectonic evolution of the northern ANS, the role of the NSS in the evolution of metamorphic complexes, and the processes in mid-crustal shear zones during Gondwanaland amalgamation.

2. Data and Methods

This study used fieldwork and satellite data to analyze the Meatiq Dome's structure. Field investigations included structural and lithological mapping, as well as collecting oriented rock samples. These ground observations were supplemented by high-resolution satellite imagery (e.g., Sentinel 2) and DEMs (Copernicus; 30m). Cross-cutting relationships between rock units provided insights into the dome's evolution. The structural data were used to reconstruct the geometry of granite plutons and infer their emplacement mechanisms, with geochronological and geochemical data supporting a new model for the dome's geometry and evolution. The microstructural analysis focused on deformed granites and mylonitic metasediments. A total of 90 thin sections were prepared to examine microfabrics in the Um Baanib pluton, oriented perpendicular to mylonitic foliation and parallel to lineation. The analysis aimed to identify deformation mechanisms and estimate temperatures assuming natural strain rates and low water content (Stipp et al., 2002a, b; Law, 2014). Magmatic and sub-magmatic fabrics were distinguished using the criteria of Paterson et al. (1989) and Vernon (2000).

3. Geological setting

3.1 Geology and Architecture of the CED

The metamorphic domes in the CED expose a structural section for the crustal architecture, which portrays the stacked fold and thrust nappes accreted through a long-lived tectonic history (>400 Ma) of subduction, accretion, and collision processes during Neoproterozoic (Greiling et al., 1994; Fritz et al., 1996; Abd El-Wahed and Attia, 2022). The crust of the CED is thought to have a tiered architecture with two structural levels (Bennett and Mosely, 1987; Greiling et al., 1994: Fig.1). The lower level, Tier 1, is comprised of amphibolite facies schists, gneisses, and mylonites, originating from various igneous and sedimentary protoliths (Andresen et al., 2010). The upper

level, Tier 2, is made up of a nappe stack of ophiolitic-Island arc sheets, which is overlain or tectonically mangled with deformed molasse basins fill (Abd El-Wahed 2010; Fowler and Osman, 2013). Ophiolitic rocks are mostly dismembered and embrace a variety of geochemical affinities inherited from their original tectonic environment, ranging from MORB setting to fore-arc and back-arc environments (Farahat 2010; Gamal El Dien et al., 2016). The contact between Tier-1 and Tier-2 is marked by a major, sub-horizontal shear zone, known as the Eastern Desert Shear Zone (EDSZ; Andresen et al., 2010). This sheared contact is exposed in the metamorphic domes as a folded mylonitic zone that detaches the amphibolite facies rocks in the core from the upper allochthonous suit (Andresen et al., 2010). It acts as a crustal-scale detachment that separates two distinct realms of different structural, metamorphic, and rheological attributes (Stern 2018). Both extensional (Fritz et al., 1996; Fowler and El-Kalioubi, 2004; Andersen et al., 2010) and thrust-related models (Sturchio et al., 1983; Mohammad et al., 2020) have been advocated to interpret the origin of these sub-horizontal shear zones. The tiered orogenic belt of CED was imperiled to several magmatic pulses that accompanied subduction, accretion, and collision stages and are manifested by a plethora of granite intrusions (Lundmark et al., 2012).

The nappe stack of CED is transected by networks of NW-trending, Km-scale transcurrent sinistral shear zones, defined by anastomosing belts of highly foliated rocks that slice up the CED into discrete blocks with complex patterns (Fig.1b). These shear zones are widely accepted as northern extensions for the NSS in the CED (e.g., Sultan et al., 1988; Fritz et al., 1996), however, their tectonic significance is still controversial (Fowler et al., 2007). The most notable NSS strands in the CED (Fig.2b) are the Atalla shear zone (Sultan et al., 1988), Hamrawin shear zone (Abuzeid, 1984), and Abu Markhat, Sibai and El-Shush shear zones (Abd El Wahed, 2008). Fritz et al., (1996) remapped these strands, suggesting they define crustal-scale shear corridors that accommodated simultaneous extensions and shortening. The pervasive NW-SE structural grain of the CED was crossed near its southern boundary by the E-W to NE-SW oriented discordant belt of Mubarak-Barramia (Shalaby et al., 2005). The belt is marked by sinistral shear zones (Wadi El-Umra shear zone; Abd El Wahed, 2014) which comprises an assemblage of highly tectonized ophiolitic rocks embedded in a matrix of well-foliated metasediments.

3.2 Geology of Meatiq Dome

3.2.1 Structural units (levels)

Meatiq area was markedly subjected to subsequent tectonic, metamorphic, and magmatic processes which, in turn, obscured most of the original lithological boundaries. The tectonic stack of the Meatiq dome is classified into two major structural units (Fig. 1b; e.g., Ries et al., 1983; Andresen et al., 2010): the Meatiq Succession and the Ophiolitic-Island Arc Succession. Meatiq Succession comprises a domed, deformed sequence of quartz- and mica-rich mylonites, schists, and less abundant amphibolite and deformed granites (Hassan et al., 2017). The mica content increases progressively, peaking in the pelitic units. The rocks of Meatiq Succession are intensely deformed with varying degrees of ductile shearing. Three thrust sheets were mapped; Um Esh El-Hamra, Abu-Zohleiqa, and Abu Fannani thrust sheets. Um Esh El-Hamra thrust sheet is the structurally lowest unit in the Meatiq dome and directly overlays the Um Baanib deformed granite. It is a highly

heterogeneous unit of quartzo-feldspathic schist, mylonites, blastomylonites with subordinate biotite-hornblende schist, and frequent concordant intrusions of mylonitic granites. Several varieties of quartzo-feldspathic rocks possess a strongly banded appearance attributed to shearing and mylonitization processes (El Gaby et al., 1984). Abu Zohleiqa thrust sheet occurs as a thick sheet composed of garnet-muscovite schist, mylonitic micaceous quartzite, and phyllonites. Abu Fannani thrust sheet constitutes a circular thrust sheet bounding and succeeding the Meatiq dome, except the northern part, and represents a conspicuous transitional unit between the amphibolite facies rocks of Meatiq Succession and overlying nappes (Fig.3). It comprises an intercalated mica- and hornblende-bearing schist and mylonites, with subordinate graphite schist. Three main varieties of amphibolites were reported in the Meatiq dome (e.g., Neumayr et al., 1996; Hamdy et al., 2017). (1) amphibolites within Um Baanib deformed granites, commonly described as "enclaves". (2) amphibolites and hornblendites intercalated with the schist and mylonites of Meatiq Succession. (3) amphibolites associated with ophiolitic rocks.

The Ophiolitic-Island arc Succession represents a complex suite of deformed, low-grade metamorphic rocks including dismembered ophiolites, ophiolitic mélange, and island-arc metavolcanics intruded by granite intrusions (Fig. 3). This assemblage is structurally intercalated with the intensely sheared molasse sediments along ASZ, west of the Meatiq dome. The ophiolites are represented by a sequence of dismembered allochthonous elongated sheets and masses of serpentinites, metagabbro, and basic metavolcanics that are disturbed by shearing. Serpentinites and associated talc carbonates are the most common ophiolitic varieties. They consist of distinct large masses and bodies encircling the Meatiq dome, oriented either east-west or north-south. Talc-carbonates occur mostly as pockets and slices near shear planes. Metagabbro and basic metavolcanics commonly occur as NW-SE trending thrust sheets, structurally overlies the serpentinites, and occur in association with hornblende schist, amphibolites, sheared serpentinites, and metasediments. The metavolcanics rocks are of andesitic basalt to basaltic composition with a tholeiitic affinity (Farahat, 2010). In ASZ, ophiolites are represented mainly by elongated sheets of variable size trending NNW-SSE, and embedded in a mélange of sheared metasediments. They are usually highly sheared, and foliated, but far from the shear zones, foliation is less pronounced.

3.2.2 Igneous intrusions

The Meatiq dome is characterized by three granitic intrusions, with ages ranging from 630.8 ± 2.0 to 590.5 ± 3.1 Ma (Andresen et al., 2009), linked to distinct magmatic events that have significantly impacted the region. These intrusions account for about 50% of the exposed area of the dome. They are categorized into the syn- to late-tectonic (Um Baanib, Abu Ziran) and post-tectonic (Arieki) plutons.

The Um Baanib pluton has an elliptical shape in the plan view and covers an area of about 120 km^2. It is principally exposed in the core of the Meatiq dome and overlain by the domed mylonitic rock units of the Meatiq Succession (Fig. 2). It consists mainly of pinkish granite and granodiorite. The essential minerals are quartz, alkali-feldspars, plagioclase, biotite, and hornblende, with a minor aegirine and riebeckite-bearing varieties reported (e.g., Ries et al., 1983; Habib et al., 1985a). Deformation is evident through penetrative mineral lineation and weak foliation, though strain intensity varies significantly. Some samples lack distinct fabrics, showing only mild

deformation or typical undeformed granite textures. The pluton also hosts amphibolite bodies, which display well-marked intrusive contacts with the granite, obliterated by subsequent thrusting (Neumayr et al., 1996). The Abu-Ziran pluton, covering roughly 19 km², comprises a variety of rock types including quartz diorite, tonalite, trondhjemite, and granodiorite. It is situated in the central and southern parts of the Meatiq dome and intrudes the Meatiq Succession and the overlying ophiolitic-Island arc Succession. Abu Ziran granitoids are composed of plagioclase, quartz, biotite, and hornblende with minor feldspar. Sericite, sphene, and opaques are the accessory minerals. They exhibit mild to intense ductile fabrics, particularly near the pluton's margins, where they parallel the foliation of the host rocks. The pluton is mainly localized near the contact between Meatiq Succession and overlying nappes and orientated parallel or sub-parallel to foliation in country rocks. The Arieki pluton is identified by its circular-shaped outcrop. It intrudes the schist and mylonites of the Meatiq Succession, as well as both Um Baanib and Abu-Ziran plutons. This post-tectonic intrusion is characterized by well-marked, irregular contacts and preserves parts of the roof rock at Gabal Meatiq, where schists and mylonites overlay the granites. The dominant rock types within the Arieki pluton are pink and pinkish-white granites and granodiorites, consisting of microcline, quartz, plagioclase, and biotite, with opaque minerals.

4. Results

4.1 Macroscopic structures and architecture of the Meatiq dome

The Meatiq dome is the key large-scale structure in the area, defined by its distinct elliptical shape. Concentric patterns and trajectories of foliation within the dome delineate two second-order, kilometer-scale domal structures (subdomes) in the eastern and western parts (Um Baanib and Um Esh El-Hamra subdomes, respectively), separated by two colinear synforms in the central region: the Abu Ziran and Abu Zohleiqa synforms (Fig. 2). The dome is intersected by various types of faults, including thrust and normal faults, with various orientations and ages.

4.1.1 Subdomes

The Um Baanib subdome is a double-plunging antiform (15 km long, 12 km wide), trending NW-SE, and defined by foliation variations around the dome's core and symmetrical repetition of units. It is cored with the oval-shaped Um Baanib pluton, which is overlain by a thick sequence of schists and mylonites. Although the contact is largely obscured by shearing and thrusting, clear intrusive contacts between the pluton and the surrounding rocks are preserved in places. The subdome has a nearly symmetrical shape with gentle to moderate dips (up to 45°), defined by the S1 foliation (supplementary 1). Stereograms of S_1 poles show a double-plunging fold with the major axis plunging NW and SE. The western continuation of the subdome is obscured by the Arieki pluton. The subdome terminates abruptly to the northwest, where extensional faults juxtapose the Meatiq Succession and ophiolitic rocks, and gradually diminishes to the south. On the other hand, the Um Esh El-Hamra subdome is a 9 km long and 4 km wide, NW-trending asymmetrical double-plunging antiform. It has a distinct elliptical shape and covers a smaller area than the Um Baanib subdome. The eastern limb dips gently (up to 30°) toward the NE, while the western limb is steeply dipping, nearly vertical (supplementary 1, 2). Stereograms of the foliation data show a well-defined girdle clustering of poles, indicating an asymmetrical fold with an inclined axial plane

striking N20°W. The fold axis plunges shallowly to SE at about 5°. The core of the subdome consists of quartzo-feldspathic schists, while the limbs are composed of phyllonites and mica-rich mylonites. The subdome dies out along the southern flank of the Meatiq dome, and the northern part is terminated by steep, step-like normal faults.

4.1.2 Synforms

The Abu Zohleiqa synform, located in the northwestern region of the Meatiq dome, trends NW-SE, and spanning ~8 km long and 3 km wide. The northern extent of the conform is truncated by the Sodemin normal fault, which diminishes further south. On the western side, an NW-trending normal fault runs parallel to the synform's axis and is accompanied by an anticline on the hanging wall. The parallelism of these fold pairs suggests a potential genetic relationship (supplementary 2). The syncline is nearly symmetrical, with limbs that dip gently, not exceeding 30°. In contrast, the Abu Ziran synform is an NW-SE trending structure, 9 km long and 4 km wide, between the Um Baanib and Um Esh El-Hamra sub-domes. Its limbs dip to the NE and SW, with average angles of 20° to 25°. Foliation data indicate a well-defined bimodal clustering in the stereogram (Fig. 2), suggesting a nearly symmetrical fold with inclined axial planes striking N20°W. A best-fit π-great circle reveals a shallowly plunging fold axis toward the SE at approximately 5°. The central and southern parts of the Abu Ziran synform are intruded by granitic sheet-like bodies from the Abu Ziran pluton. This synform and its intrusions have been affected by various thrust and normal faults of differing orientations (supplementary 2). Notably, the southern extent of the synform terminates abruptly due to normal faults that juxtapose Meatiq Succession with ophiolitic nappes.

4.1.3 NW-SE-striking thrust faults

Meatiq Succession and overlying nappes were dissected by several NNW-SSE-striking thrust faults, that dip both NE and SW. These thrust faults are well exposed east of the Um Baanib sub-dome, along Wadi Murr, where several thrust faults are cutting across the quartzo-feldspathic units (Fig. 3a, b). These faults are arranged in closely spaced, large-scale imbricated duplexes with variable displacements. Similarly, a system of thrust faults duplexes cut across the deformed granites of Um Baanib (Fig. 3c, d) and Abu Ziran plutons. Notably, an arcuate-shaped fault crosses Um Baanib granite and runs for about 10 Km along its eastern contact. This fault structurally juxtaposes Um Baanib deformed granite with amphibolites in several localities. On the road of Qift-Quseir, a typical example of a thrust duplex is well-preserved in Abu-Ziran granite. A zone of mylonitization and brittle fracturing marks the floor thrust. Several fault planes are curved and characterized by the staircase geometry causing the bending of hangingwall rocks along the thrust plane. Slip lineation on fault planes and the vergence of thrust faults indicate a major W-to-SW-tectonic transport. In ASZ, these faults display an imbricated thrust duplex system, that marks the contacts of different units.

4.1.4 Normal faults

The Meatiq dome is characterized by a complex network of intersecting normal faults with varying

orientations: NE-SW, WNW-ESE, and NW-SE. The oldest of these trends, NE-SW, is marked by a pervasive set of steep fault planes, generally dipping around 70°. An example is the Sodemin fault along the northern flank, which juxtaposes ophiolitic nappes with the Um Baanib pluton and Meatiq Succession (Fig. 3e). This fault truncates both ductile fabrics and thrust faults at high angles, and is accompanied by several sub-parallel faults exposed north of the dome. The Abu Ziran fault transects the southern limb, juxtaposing ophiolitic nappes with the Meatiq Succession, though its continuity to the east is uncertain. The lack of kinematic markers complicates displacement estimates, which range from tens to hundreds of meters. This fault set is not restricted to the dome borders; it also transects the dome's interior with multiple steep faults, indicating a pervasive extensional system rather than localized faulting along the dome's edges. The clear cross-cutting relationship between these faults and the Arieki Pluton, suggests a post-orogenic extensional phase. The other younger WNW-ESE and NW-SE trending faults and fractures exhibit cross-cutting relationships with older sets of faults and are likely associated with Phanerozoic rifting events.

4.1.5 Architecture and geometry of Meatiq dome

Seven geological cross-sections were constructed to illustrate the dome's internal structure and relationships between subdomes, synclines, and different fault sets (Fig. 4). Section A-A', which transects the southern region of the Meatiq dome, offers a representative portrayal of its structural elements. The two subdomes and the intervening Abu Ziran synform are clearly distinguished by the dip of foliation observed along their flanks. The Um Baanib subdome is dissected by a series of thrust faults trending NW-SE, and dipping due NE. Notably, amphibolite enclaves are predominantly associated with these thrust contacts. In contrast, the neighboring Um Esh-El-Hamra subdome exhibits a highly asymmetric shape, with a western near-vertical limb. This limb is attenuated along the ASZ, where the rocks steepened and tectonically mixed with ophiolitic nappes. The Abu Ziran pluton intrudes the Abu Ziran synform parallel to the contact between the Meatiq Succession and ophiolitic nappes. In contrast, the alkali granites intruding Abu Ziran pluton display a distinct sharp vertical intrusive contact, indicative of differences in geometry and emplacement style. The dome is truncated by the sub-vertical sheared belt of the ASZ along its western side. Additionally, it is intersected by steep normal faults, some of which exhibit significant displacement. Section B-B'. shows a similar configuration to the preceding section, albeit with the presence of the Arieki pluton, which obscures the western limb of the Um Baanib subdome. The orientation of the thrust faults within the pluton changes, aligning north-south. Section C- C' illustrates the fading of the Um Esh El Hamra subdome and the Abu Ziran synform, replaced further northward by the Abu Zohleiqa synform/antiform pairs. The eastern flank of this synform is demarcated by a steep NW-SE oriented normal fault that dips NE, representing an abrupt change in the dip of the foliated rocks within the Meatiq Succession. On the other side, the NW-SE trending cross sections provide a clear depiction of the diminishing subdomes and synforms along the borders of the dome. Sections (D-D') and (E-E') show the gradual dipping of the southern flanks of the Um Baanib subdome, as well as the abrupt attenuation of the entire structure along the Sodemin normal fault in the north. Section (F-F') shows the intrusive contacts of the Arieki pluton with the Um Baanib subdome. The pluton is transected by a series of NE-SW-trending, steeply dipping normal faults. Section G-G' elucidates the longitudinal geometry of the Um Esh El-Hamra subdome, which is characterized by a moderate dip along its southern limb, and

shallow dipping on the northern limb. The subdome is dissected by several normal faults, resulting in a distinct step-like geometry.

4.2 Mesoscopic structures of Meatiq dome

4.2.1 Mesoscopic structures of Meatiq Succession

The Meatiq Succession rocks display pervasive tectonic fabrics, mainly LS-tectonites, with localized mylonitic zones, shear bands, boudinage, and intrafolial folds. Deformation intensity varies, with strain localization along certain horizons and lithological differences. Primary structures are largely obliterated by ductile shearing and metamorphism. Tectonic foliation (S_1) is widespread, typically aligned parallel to lithological contacts, and defined by the orientation of mica, amphiboles, and stretched quartz and feldspar (Fig. 5a). Near Um Baanib pluton, quartzofeldspathic schist was intruded by mylonitized granite sheets, creating distinctive banding (Fig. 5b). Mylonitic foliation is less frequent and localized along sheared contacts. Competent lithologies are deformed into tectonites with attenuated, transposed lensoidal layers and tight or isoclinal folds (Fig. 5c, d). A penetrative mineral lineation (L_1) is present in deformed granites and metasediments (Figs. 5e, f), characterized by stretching crystals and ribbons, or alignment of mafic clusters and clots, and mostly plunges to NW. The succession also exhibits diverse boudinage structures in quartz veins and felsic intrusions, particularly where competent and non-competent lithologies contrast. Boudin types include torn, drawn, pinch-and-swell, and shear bands. Asymmetrical, sigmoidal boudins with pressure shadows are observed, indicating shearing with top-to-NW sense (Figs. 5i, j). These boudins are common in highly attenuated horizons, indicating significant shearing along structural contacts (Fig. 5h). Additionally, foliation boudins are visible in competent lithologies like quartzo-feldspathic schist (Fig. 5k).

Mesoscopic folds are ubiquitous and exhibit various styles and orientations with a dominance of close overturned and recumbent folds (Fig. 6a). The lithological contacts and tectonic fabric are strongly folded around axes that plunge ~10° toward the N60°E direction, perpendicular or oblique to the L_2 lineation. However, folds with a high angle to the stretching lineations were also documented. Several fold styles have been observed in the Meatiq Succession. The first style is harmonic, tight-to-close recumbent folds with curved to subangular hinge zones (Fig. 6b). These folds are well-developed in quartz-feldspathic and mica schist. The quartzofeldspathic-rich domains act as highly competent layers, while the mica-rich domains act as incompetent layers that deform and flow to accommodate the spaces (Fig. 6c, d). Another fold style is observed in schists, where alternating widely spaced thin mica-rich and felsic (quartz and feldspar) horizons display folds with tight to isoclinal angles (Fig. 6e). These folds exhibit thickened hinges and thinner, stretched, and boudinaged limbs. Intrafolial folds aligned parallel to the pervasive foliation, are typically tight to isoclinal and asymmetric, with axial surfaces trending NE-SW, gently dipping due SE, and verge toward NW. Kink bands and crenulation folds with sharp hinges and asymmetrical straight limbs are observed in highly foliated pelitic varieties. The sense of fold asymmetry is consistent with a top-to-NW shear sense. Additionally, sheath folds with noses parallel to mineral lineation were observed at various scales. They are asymmetrical with highly

curved axes parallel to the lineation. Sections normal to the fold axes display a distinctive eye-shaped pattern (Fig. 6f).

4.2.2 Mesoscopic structures of ophiolitic-island arc Succession

The ophiolitic nappes and associated metavolcanics display multiple generations of structures. The oldest phase includes NE-SW trending thrust faults, along with less frequent penetrative foliation, folds, and boudinage structures, particularly evident along contacts within the ophiolitic nappe south of the Meatiq dome. Kinematic indicators suggest a top-to-NW transport direction, consistent with observations in the fabrics of Meatiq Succession. In ASZ, another generation of penetrative foliation and lineation is present, likely related to a transpressional shearing event. This sub-vertical foliation (S_2), predominantly trending NW-SE, aligns with the shear zone's orientation, while the lineation (L_2) is mainly sub-horizontal, paralle to foliation. Additionally, L_2 slip lineations along NW-SE striking thrust faults indicate tectonic transport predominantly to SW.

4.2.3 Mesoscopic structures of amphibolites enclaves

The amphibolite bodies in the Um Baanib pluton bear a variety of tectonic fabrics believed to represent the oldest structural generation in the CED (Loizenbauer et al., 2001). These rocks exhibit conspicuous tectonic foliation and lineation, marked by the alignment of hornblende, biotite, and plagioclase crystals. The planar and linear fabrics were folded around an axis that plunges southeast (El-Gaby et al., 1984). However, other studies disregarded the orientations of these structures, given that the amphibolite enclaves may have undergone reorientation during the emplacement of the pluton (Loizenbauer et al., 2001). The origin of these tectonic fabrics in the amphibolites and their temporal relationship to the mylonitic fabrics in the Meatiq Succession will be discussed later.

4.3 Microstructural anatomy of Meatiq dome

4.3.1 Microstructures of Um Baanib deformed granite

The Um Baanib Pluton records progressive deformation, ranging from sub-magmatic structures formed during melt crystallization to high- and low-temperature solid-state deformation and brittle shearing. The deformation intensity increases near the contact with thrust sheets, while the pluton's inner areas retain undeformed igneous textures. The granite displays "magmatic-looking" fabrics overprinted by mylonitic, solid-state deformation, suggesting coeval deformation and melt emplacement. Magmatic foliation and lineation are preserved through aligned albite twinning in anhedral to subhedral plagioclase crystals with lobate to serrate boundaries (Figs. 7a-d). These perfectly aligned crystals reflect an earlier magmatic Shape Preferred Orientation (SPO) of plagioclase, later overprinted by high-temperature recrystallization of the crystal margins. Some crystals retain straight faces and elongation parallel to albite twinning, implying that these aligned crystals refer to original magmatic foliation (Paterson et al., 1989). This interpretation is supported by: (1) the preservation of well-aligned euhedral plagioclase crystals preserved within large K-feldspar crystals, showing a poikilitic texture (Fig. 7e). These euhedral crystals, shielded by K-feldspar oikocrysts, preserving the original magmatic deformation. (2) Zoning patterns in some

crystals, indicative of magmatic origin. (3) the high temperatures (>450°C) required for dynamic recrystallization of feldspars (Tullis, 1983; Paterson et al., 1989).

K-feldspar occurs as subhedral to anhedral crystals, often exhibiting flame-shaped perthites (Fig. 7f). Plagioclase shows signs of dynamic recrystallization through serrated margins, indicating high-temperature deformation (Fig. 7g). Quartz forms elongated crystals, aggregates, or ribbons with prominent SPO aligned parallel to the main fabric (Figs. 7h, i). Grain boundaries are highly sutured and serrated, suggesting dynamic recrystallization by high-temperature Grain Boundary Migration (GBM; Passchier and Trouw, 2005). Biotite and amphibole align as aggregates and laths, however, discerning whether the alignment is magmatic or tectonic is challenging. C-S fabrics and shear bands are widely observed near pluton contacts and align with magmatic microstructures' orientation and shear sense. No evidence of a hiatus exists between sub-magmatic and high-temperature solid-state deformation. Instead, fabrics show a gradual transition, indicating persistent deformation from hypersolidus to subsolidus conditions (Zibra et al., 2012). This indicates that the granite experienced magmatic deformation in the presence of melt, which occurred synchronously with regional deformation.

In addition to the submagmatic fabrics, the granites exhibit two additional categories of solid-state deformation: low-temperature ductile fabrics and brittle microstructures. The low-temperature fabrics are represented by the undulose extinction in some Quartz crystals (Fig. 7j), indicating solid-state ductile deformation at relatively low temperatures. Brittle microstructures: Near brittle thrust faults, granite often exhibits brittle microstructures, such as (1) cataclastic shear zones, and (2) fractured and microfaulted plagioclase crystals (Fig. 7k, l). Cataclastic zones, cutting across ductile fabrics, are 0.5–2 mm wide and consist of extensively fractured and pulverized crystals. The fracturing of quartz and feldspar grains suggests deformation at low temperatures not exceeding 300 °C (Tullis 1983). These brittle microstructures likely represent a distinct phase of deformation that occurred after the earlier fabrics.

4.3.2 Microstructures of Meatiq Succession

The analysis of the mylonitic varieties in the Meatiq Succession indicates a prevalent crystal plastic deformation, influenced by a strong non-coaxial strain component. The eastern transect of the dome offers the best-preserved section, providing insights into microstructural evolution and variations in rock types (Fig. 8a). Notably, the microfabric profile demonstrates a dramatic down-section increase in the deformation temperature (Fig. 8b, c). Deformation intensities vary markedly along the section, reflecting strain partitioning due to differences in mineral composition, abundance of weak phases (e.g., mica), and rheological properties.

Adjacent to Um Baanib pluton, rock varieties exhibit a spectrum of compositions ranging from quartzo-feldspathic mylonites to quartzites, phyllonites, and some pelitic varieties such as biotite schist. Quartzo-feldspathic varieties (samples Mt-18 & Mt-16) typically display a weak foliation, except for those rich in mica content, where both quartz and feldspars occur as stretched crystals exhibiting dynamic recrystallization. Quartzites and quartz-rich tectonites (Mt-13& Mt-14) are characterized by a pronounced grain-shaped foliation, delineated by elongated quartz ribbons (Fig. 9a) with sutured and serrated boundaries, indicative of GBM (Figs.9b, c). The peak metamorphic assemblage, marked by sillimanite, garnet, biotite, and hornblende, aligns with high-temperature

metamorphic conditions. White mica fishes, abundant in this unit, exhibit well-developed sigmoidal shapes and are arranged in a characteristic S-C fabric (Fig. 9d). Additionally, pinning and dragging microstructures are prevalent where quartz contacts mica grains. Some deformed quartz grains exhibit a locally developed chessboard extinction feature (Fig. 9e), constraining the minimum deformation temperature in this zone to ~630°C (Law 2014). Quartz grain sizes are influenced by mica content: mica-poor rocks show quartz ribbons and larger grains with GBM (Figs. 9f, g), while mica-rich phyllonites exhibit anhedral quartz with weaker GBM (Fig. 9h). This can be attributed to strain accommodation by the basal slip system in the weaker, easily deformed mica, which inhibits the development of SPO in quartz (e.g., Hunter et al., 2016, 2018). In some samples, foliation domains are slightly anastomosing around lensoidal-shaped microlithons (Fig. 9f). Some quartz grains display undulose extinction, indicating a subsequent low-T ductile deformation.

In the upper pelitic units, mylonitic biotite schist (Mt-14& Mt-13) and amphibolites prevail as dominant rock types. These varieties comprise polymineralic sheared pelitic rocks with abundant feldspar porphyroclasts embedded in a highly anisotropic matrix of quartz, biotite, muscovite, and feldspar grains. These clasts exhibit strain shadows of mica bands and, in some cases, fine-grained recrystallized mantles. The alignment of mica flakes and aggregates defines the foliation. Quartz grains in these varieties occur as small, anhedral equant grains within the matrix (Fig. 9i), showing weak preferred orientation and straight extinction. These features suggest strain-free recrystallized quartz grains formed through subgrain rotation recrystallization (Hirth and Tullis 1992). These features, typical of brittle-ductile transitions, imply deformation temperatures of ~450°C (Tullis, 1983; Hirth and Tullis, 1992; Law, 2014) with dominant dislocation creep. The mylonites contain distinct generations of garnet porphyroblasts. The first comprises elongated crystals parallel to lineations, interpreted as pre-kinematic growth. The second generation is characterized by elliptical to irregular-shaped crystals enclosing crenulated or spiral-shaped quartz inclusions, that are misaligned to the external foliation (Fig. 9j). This generation is interpreted to have grown syn-kinematically. A third generation, restricted to Abu Ziran Pluton country rocks, comprises euhedral to subhedral crystals cutting across foliation, likely formed during metamorphic events concurrent with waning deformation or after it (Mohammad and El Kazzaz, 2022). The kinematic indicators within the MSZ support a top-to-NW tectonic transport (Fig. 9k, l).

5. Discussion and Implications

5.1 Structural nature of metamorphic dome in CED: Are they extensional MCCs?

Dome-shaped complexes in the ANS are often classified as either mantled gneiss domes (El Gaby et al., 1984) or extensional MCCs (Fritz et al., 1996; Blasband et al., 2000). Gneiss domes, typically cored by migmatites, orthogneisses, and granites with a mantle of high-grade schist and gneiss, are thought to form through buoyant flow and diapirism (Eskola, 1949; Teyssier and Whitney, 2002; Whitney et al., 2004; Yin, 2004). Alternative models emphasize structural mechanisms such as interference folding, fault-related folding, and ductile crustal flow (Boyer and Elliott, 1982; Yin, 2004; Godin et al., 2006; Cao and Neubauer, 2016; Jessup et al., 2019). Conversely, MCCs, initially defined in the North American Cordillera (Coney, 1980; Lister and Davis, 1989), involve dome-shaped structures of deeply exhumed crustal rocks surrounded by upper crustal rocks and cut by

low-dipping normal faults linked to regional detachment faults (Buck, 1988; Wernicke, 1995). This model has also been applied to other extensional systems, such as the Aegean Sea (Forster and Lister, 1999), and many ancient gneiss domes in orogenic belts have been reinterpreted as MCCs formed during post-orogenic extension (Mancktelow and Pavlis, 1994; Wawrzyniec et al., 2001). Based on the definitions provided, the Meatiq dome cannot be classified as an MCC, despite exhibiting several similar characteristics, for following reasons:

1) MCCs typically develop in extensional settings, associated with low-angle normal faults and sub-horizontal detachments (Lister and Davis, 1989). Such structures are absent in the Meatiq dome and other domes in the CED and Sinai (Fowler and Osman, 2001; Fowler et al., 2007). Instead, high-angle normal faults along the Meatiq dome's flanks intersect the ductile fabrics of the Meatiq Succession and the post-kinematic Arieki pluton. The steep dip of these faults, their interaction with ductile fabrics, and the timing discrepancies between normal faulting (<590 Ma) and shearing activity (>630- ~600 Ma) strongly counter this model.
2) The complex structure of the subdomes and folds in the Meatiq dome, including the asymmetry of the Um Esh El Hamra subdome and the geometrical relationship between brittle thrust faults and subdomes cannot be explained by isostatic rebound and uplift. Instead, these folding and thrusting patterns indicate a later shortening event distinct from the earlier NW-ward shearing.
3) The $^{40}Ar/^{39}Ar$ dating of hornblende and mica from the amphibolites and metasediments of the Meatiq Succession show cooling from 500°C to 350°C during 587-579 Ma, suggesting rapid regional exhumation linked to extensional tectonics (Fritz et al., 2002). However, this age does not align with the timing of the sub-horizontal shearing in the Meatiq dome, which ceased ~600 Ma (Andresen et al., 2009, 2010). This significant disparity indicates that exhumation postdates shearing and is likely linked to a distinct event following the orogeny and dome formation.

The Meatiq dome also doesn't fit the typical definition of a gneiss dome, which typically features cores composed of migmatites and gneisses. Unlike metamorphic domes in Sinai (Hassan et al., 2021) and the Southern Eastern Desert (e.g., Migif-Hafafit; Fowler and El Kalioubi, 2002; El Kazzaz, 2009), the Meatiq dome lacks migmatites, indicating a limited partial melting and buoyant flow, and thus challenges the role of thermal buoyancy and flow as a mechanism of doming. Instead, a broader definition of gneiss domes, accommodating diverse mechanisms, better applies to the metamorphic domes in the CED. Based on structural data from the Meatiq dome (Fig. 10), we suggest that the domed complexes of the CED represent highly sheared, mylonitic mid-crustal domains formed through NW-directed tectonic transport of thrust nappes. These sub-horizontal shear zones underwent a subsequent shortening phase, resulting in the observed dome/fold geometry. This multi-phase deformation history aligns with Yin's (2004) broader framework, defining gneiss domes as products of varied mechanisms and processes.

5.2 Geometry and emplacement mechanism of Um Baanib pluton

5.2.1 Pre-tectonic vs. Syn-tectonic emplacement

The Um Baanib pluton has traditionally been interpreted as a pre-tectonic intrusion, emplaced before NW-directed tectonic transport (Fritz et al., 1996; Loizenbauer et al., 2001; Andresen et al., 2010). This envision considers the pluton as the lowest exposed structural unit, with the contact

between the granite and overlying units representing a crustal-scale shear zone (Andresen et al., 2010; Abu Sharib et al., 2019). It suggests the pluton was emplaced ~631 Ma in an island-arc setting, followed by rapid denudation and subsequent tectonic transport (>609–605 Ma) that placed mylonitic metasediments and ophiolitic nappes over the exposed rocks, including the Um Baanib pluton. In contrast, our study provides compelling pieces of evidence for the syn-tectonic emplacement of the pluton along the MSZ: (1) The Um Baanib pluton shows clear intrusive relationships with the overlying metasediments, manifested as tabular intrusions within schists and mylonites, confirming the existence of metasediments before the granite's emplacement. These intrusions display significant ductile deformation, with fabrics akin to those in the host rocks, indicating contemporaneous deformation. (2) The granite exhibits sub-magmatic fabric, marked by aligned plagioclase crystals, overprinted by high-temperature solid-state deformation, including GBM recrystallization and mylonitic fabrics. This transition from magmatic to solid-state deformation supports a syn-kinematic emplacement. (3) Microstructural analysis of the mylonitic metasediments near the pluton reveals high-temperature deformation fabrics that transition to lower-temperature fabrics up section. This gradient may suggest progressive ductile deformation within the pluton's contact aureole, resembling metamorphic anomalies associated with syn-tectonic intrusions in the western United States (e.g., Law et al., 1992; Nyman et al., 1995; Morgan and Law, 1998; Heaverlo, 2014). Collectively, these lines of evidence endorse the syn-kinematic emplacement.

5.2.2 Geometry and emplacement mechanism

At its current exposure level, the pluton exhibits an elliptical shape in plan-view, trending NW-SE, and primarily exposed in the core of the Um Baanib sub-dome. However, the exposures extend to the west, suggesting a subsurface extension of the pluton beneath the mylonitic metasediments. Since its emplacement, the pluton has experienced multiple stages of deformation, significantly modifying its original geometry through successive generations of overprinting structures. Nevertheless, we developed an approximate reconstruction of the pluton's initial shape and emplacement mechanism based on two key observations: (1) The pluton's contacts with overlying units and the amphibolites align with tectonic fabrics. (2) The Meatiq Succession, particularly along the eastern flank of the dome, contains several concordant sheet-like intrusions similar to the Um Baanib granite. These sheet-shaped intrusions are emplaced parallel to the mylonitic foliation. Similar intrusive sheets are observed within the amphibolites (supplementary 3). These characteristics—parallelism of pluton contacts with the wall rock fabric and the presence of granite sheets in adjacent rock units—are typical of tabular intrusions emplaced along shear zones documented worldwide (e.g., Hutton et al., 1990; Petford et al., 2000). These plutons are often aligned parallel to fabrics in the shear zone walls, and shaped by inherent weaknesses (Hutton 1992, 1996). Similar features are reported in the Abu-Ziran pluton, known for its sheet-like geometry (Mohammad and El Kazzaz, 2022). Despite the lack of conclusive evidence, we approximate the shape of the Um Baanib pluton, at the time of emplacement, as a sheet-shaped intrusion within a sub-horizontal shear zone (supplementary 3). Space for the pluton was likely created by shearing, with granitic magma ascending through unexposed feeder dykes and spreading laterally along the shear zone. Crystallization during emplacement developed magmatic

fabrics influenced by regional stresses. Post-emplacement, subsequent shortening, and extensional phases further altered the pluton's geometry.

5.2.3 The geometry of amphibolites within Um Baanib granites: enclaves or thrust sheets

The Um Baanib pluton hosts amphibolite bodies, often described as enclaves (Neumayr et al., 1996), exhibiting gneissic banding, folding, and localized migmatization. These features are linked to an early tectono-metamorphic phase (M1/D1) (Loizenbauer et al., 2001). Geochemical analysis confirms their igneous origin, with mafic composition, formed in two regimes: Mid-Ocean Ridge (MOR-type) and within-plate basaltic magmatism (Neumayr et al., 1996, 1998). Age estimates range from 1.14 Ga to 800 Ma (Loizenbauer et al., 2001). The current findings cast some doubt regarding their nature, and whether these amphibolites are randomly distributed enclaves or thrust sheets co-located with the thrust faults dissecting the pluton. Key observations include: (1) Clear intrusive contacts between the Um Baanib granite and the amphibolites. At the outcrop scale, deformed granitic sheets intrude parallel to the pronounced foliation in the amphibolites. (2) These intrusive contacts are disrupted by thrust faults that enclose the amphibolites as thrust sheets and truncate earlier intrusive relationships. (3) Satellite imagery shows that amphibolites occur as belts of sheet-like bodies striking N40°W, N-S, and N30°E, parallel to the thrust faults (supplementary 4). (4) Ductile fabrics in the amphibolites resemble those in the deformed Um Baanib granite and the overlying schists and mylonites. Foliation, and stretched lineation in the amphibolites align with those in the Meatiq Succession. Moreover, the dominant fold trends within the amphibolites, ranging from ENE-WSW to ESE-WNW, neatly align with those documented in the Meatiq Succession. El Gaby et al. (1984) also documented fold axis plunging ESE (10-15°). This consistency in structural features strongly suggests a shared deformational history. Amphibolites within the Um Baanib granites are interpreted as thrust sheets, likely representing an underlying rock unit exposed during thrusting. Unlike expected random shapes, distributions, and orientations of enclaves, amphibolites are structurally controlled by thrust faults, influencing their shape, and spatial distribution.

In addition, the high-grade metamorphism and complex deformation of the amphibolites have been reassessed in light of our findings. While earlier interpretations linked the amphibolite fabrics to a distinct tectono-metamorphic phase, the observed similarities with the Um Baanib granite and Meatiq Succession fabrics. In addition, the migmatization in amphibolites appears to be localized, with most of the rocks exhibiting intense foliation. These findings challenge the idea of a distinct deformation phase, suggesting that amphibolite fabrics result from the NW-directed tectonic transport event, like the fabrics in the surrounding rocks. Localized migmatization in amphibolites is likely tied to the thermal influence of the Um Baanib pluton’s emplacement.

5.3 Structural evolution model of Meatiq dome

This section presents a revised model for the structural evolution of the Meatiq dome, which has broader implications for CED and northern ANS. The model is supported by published geochronological and geochemical data, identifying four key Precambrian deformation phases (D_1 to D_4), spanning the breakup of Rodinia (~1 Ga) to the Gondwana assembly (650–550 Ma). D_4

represents widespread rifting in the northern ANS, likely extended to the beginning of Paleozoic, with later Phanerozoic extensional phases driving ANS exhumation and exposure.

5.3.1 D_1 phase: extensional tectonics and Rodinia breakup (~1 Ga)

The earliest deformation phase (D_1) was extensional, likely related to the breakup of Rodinia (~1 Ga; Fowler and Osman, 2001). Although direct extensional structures remain unidentified, the 1.10–1.03 Ga rift-related metavolcanics and mafic intrusions in Sinai (Be'eri-Shlevin et al., 2012) provide indirect evidence of this stage. The lithological characteristics and bimodal composition of these rocks support continental rifting settings (Hassan et al., 2014). In the Meatiq dome, geochemical analysis of amphibolite sheets in the Um Baanib pluton suggests origins in two tectonic settings: within-plate and MOR (Neumayr et al., 1996). Dated amphibolites (1.14 Ga - 800 Ma; Loizenbauer et al., 2001) overlap with rift-related rocks in Sinai and ophiolitic nappes in the ANS (880-690 Ma; Stern, 1994). These amphibolite sheets may represent remnants of rift-related volcanics or oceanic lithosphere from later seafloor spreading, though further study is required.

5.3.2 D_2 phase: NW-directed tectonic transport and MSZ formation (>631– ~600 Ma)

The D_2 deformation in the Meatiq dome is characterized by various shear zone-related fabrics, including pronounced foliation, stretching lineation, and intrafolial folds, which are typically aligned parallel or at low angles to lithological contacts (Sturchio et al., 1983; Andresen et al., 2010). Similar structural features have been documented in other metamorphic domes in CED, such as Um Had (Fowler and Osman, 2001), El-Sibai (Fowler et al., 2007), and El-Shalul (Ali et al., 2012). Restoring these ductile fabrics to their pre-doming/ folding orientation reveals a sub-horizontal shear zone with a top-to-NW sense of shear, referred to as EDSZ (Andresen et al., 2010). Key kinematic markers suggest NW-directed tectonic transport, attributed to either extensional (Fowler and El Kalioubi, 2004; Andresen et al., 2010) or compressional (Mohammad and El Kazzaz, 2022) regimes. We adopt a compressional model for this shear zone, linking it to NW-verging thrust faults formed during ophiolitic nappe stacking in CED. The term MSZ is preferred due to uncertainties regarding EDSZ continuity beneath the CED and whether the exposed shear zones in the domes represent a single regionally significant shear surface or multiple synchronous shear zones.

The timing of D_2 phase is constrained by pluton ages, with shearing initiating before the Um Baanib pluton emplacement and persisting with mild deformation during the Abu Ziran pluton emplacement, indicating activity before 631 Ma. The age of the El Shalul pluton, which shares similarities with the Um Baanib pluton, could expand the shearing age to >634 Ma (Ali et al., 2012). Late to post-tectonic plutons, such as Fawakhir (598 ± 3 Ma) and Um Had (596.3 ± 1.7 Ma), unaffected by D_2, set its cessation at ~600 Ma (Andresen et al., 2009). This time aligns with the age of amphibolite facies metamorphism (625 ± 5 Ma) in the Um Had complex (Abu Sharib et al., 2019), interpreted as contemporaneous with D_2 shearing (Fowler and Osman, 2001; Abu Sharib et al., 2019). The timing of the D_2 phase aligns with the ages of the Hammamat molasse sediments (Fowler and Hamimi, 2021), suggesting a potential link. We interpret that these sediments were deposited in a series of foreland and piggyback basins ahead of NE-SW trending thrust nappes,

where advancing nappes shed eroded sediments into the basin.

5.3.3 D_3 phase: E-W transpression and domes formation (~605–596 Ma)

During this phase, the tectonic regime in the northern ANS shifted to NE-SE to E-W transpression, likely driven by the oblique convergence of East and West Gondwana (~605–596 Ma; Andresen et al., 2009; Abu Sharib et al., 2019). Compression during this stage produced map-scale NW-trending folds and thrust faults, deforming early-stacked nappes across the CED (Greiling et al., 1994; Johnson et al., 2011). Key structures include extensive fold-and-thrust belts in the Hammamat molasse basins (Abdeen and Greiling, 2005) and prominent large-scale folding in the gneiss domes (Mohammad et al., 2020). In the Meatiq Dome, the MSZ and associated D_2 fabrics were folded into their present architecture, forming two subdomes separated by an intervening synform. On the other hand, the wrench component of this phase is manifested by a system of NW-SE trending faults (NSS), which cut across the CED, disturbing the early-formed nappes, and associated Hammamat molasse basins. Kinematic and vorticity analyses from the ASZ reveal a sinistral general shear zone with a nearly equal contribution of pure and simple shear (Mohammad et al., 2020).

5.3.4 D_4 phase: post-orogenic extension (<591- 540 Ma)

Following the assembly of Gondwanaland, a phase of intense post-orogenic magmatism occurred, characterized by the intrusion of alkaline granites (e.g., Um Had and Arieki plutons), dated to 600–550 Ma (Johnson et al., 2011; El-Bialy, 2020). Concurrently, significant crustal extension (D_4) affected the northern ANS, primarily in the NW-SE direction, with additional stretching in the N-S and E-W directions (Johnson et al., 2011). Evidence includes NE- to ENE-trending faults cutting through orogenic nappes, shear zones and post-orogenic intrusions. In the Meatiq dome, this phase is defined by pervasive NE-trending, steep normal faults affecting all rock units, including the Arieki pluton, constraining this extensional phase to an age of <591 Ma. Regionally, it is marked by extensional features such as bimodal dyke swarms across the northern ANS, dated to 591–540 Ma (Jarrar et al., 1983; Stern et al., 1984; Genna et al., 2002; Jarrar et al., 2004). While orientations vary, most dykes trend eastward, with additional N-S and NW-SE trends (Johnson et al., 2011).

5.3.5 Phanerozoic rifting events

The exposed basement rocks of the northern ANS display a range of brittle faults with orientations that don't align with Neoproterozoic stress fields. Instead, these faults resemble structures typically associated with Phanerozoic sedimentary cover, suggesting a connection to later deformation phases. Extensional tectonism largely shaped the Phanerozoic tectonic history of the region, beginning with Cretaceous rifting (~145–100 Ma) driven by the opening of the South Atlantic Ocean. This phase formed WNW-ESE to NW-SE trending rifts, such as the Kharit-Hodein graben (Mostafa et al., 2023), and was accompanied by magmatic activity, including ring complexes and Natash volcanics (Moghazi et al., 1997; Surour et al., 2024). In the Meatiq dome and CED, some extensional faults follow WNW-ESE trends, aligning with these rifts. During the Tertiary, the divergence of Africa and Arabia drove the formation of the NNW-SSE trending Red Sea rift,

uplifting and denudation of the sedimentary cover, and exposure of the ANS along rift shoulders. Thermochronometric data suggest rifting began at 24–23 Ma, with rift shoulders emerging at 22–20 Ma (Steckler and Omar, 1994; Omar and Steckler, 1995).

5.4 Origin of domiform geometry of the Meatiq complex

The analysis of the Meatiq area reveals a complex geometry featuring a double-dome structure with two second-order sub-domes separated by synforms and modified by a network of thrust and normal faults. Any model explaining the dome's origin must account for (1) the geometry of the Um Baanib pluton to infer its emplacement mechanism, (2) the spatial and temporal relationships between the sub-domes and associated faults, and (3) the geometric characteristics of the sub-domes. This study introduces a new model for the Meatiq dome's evolution and the mechanisms driving its formation.

5.4.1. Um Baanib subdome

The origin of the Um Baanib subdome has been debated, with early models attributing its formation to diapirism (Ries et al., 1983; El Gaby et al., 1984). However, the absence of structural features such as radial lineations and flattening strain patterns casts doubt on these models. Later, Habib et al. (1985a, b) linked the doming to folding during distinct orogenic events, while Bennett and Mosley (1987) identified the domes as imbricate antiforms forming a duplex structure. More recently, the extensional MCCs model has been widely proposed for gneiss domes in the northern ANS (Fritz et al., 1996; Blasband, 2000; Andresen et al., 2010), attributing doming to isostatic rebound and crustal upwelling triggered by low-angle normal faulting. Our interpretation of the Um Baanib pluton as a syn-kinematic intrusion, emplaced as a tabular sheet along the MSZ without evidence of forceful intrusion, challenges the diapiric model. The limited occurrence of migmatites in the subdome’s core suggests localized melting linked to pluton emplacement, contradicting the thermal and gravitational upwelling model for doming. Furthermore, the absence of low-angle normal faults or detachment surfaces in the Meatiq Dome and the surrounding CED casts doubt on its classification as MCC and questions the role of isostatic upwelling in dome formation.

Here, we provide an alternative interpretation for the origin of the Um Baanib subdome as a result of the antiformal stacking of thrust sheets over a non-exposed ramp. The current work reveals the presence of a series of thrust duplex structures in the Meatiq Succession, as well as the Um Baanib and Abu Ziran plutons. These thrusts truncate the ductile fabrics and manifest as NW-SE-oriented thrust sheets, running parallel to the Um Baanib subdome's major axis. They are mostly dipping either NE or SW, with a prevailing SW-ward tectonic transport, directed towards the foreland. The thrusts truncate ductile fabrics and exhibit arched map-scale traces, delineating amphibolite bodies. This pattern is consistent with antiformal stacking in culminations and window structures of thrust belts (e.g., Boyer and Elliott, 1982; McClay, 1992; Mitra et al., 2010). This mechanism suggests that folding and bulging of the sheared rocks of Meatiq Succession rocks resulted from sequential thrust propagation and stacking (Fig. 11a). The alignment between thrust faults and the subdome’s orientation, along with arched fault traces, strongly supports the antiformal stacking model over alternative interpretations. In addition, this model accounts for the distribution and geometry of the amphibolite sheets in the Um Baanib pluton, and their interpretation as thrust sheets. Antiformal

stacking has been widely applied to the formation of gneiss domes associated with thrust duplexes in various fold-thrust belts (Yin, 2004; El Kazzaz, 2012; Shoorangiz et al., 2019; Jessup et al., 2019).

5.4.2 Um Esh El-Hamra subdome

The Um Esh El-Hamra subdome is a double-plunging antiform with an elliptical shape, elongated NW-SE, and spans 9 km in length and 4 km in width, giving it an aspect ratio of 2.25. This contrasts with the Um Baanib subdome, which has a lower aspect ratio (1.25), suggesting different doming mechanisms. Analysis of the Um Esh El-Hamra subdome reveals features typical of fault-related folds: (1) a gently dipping backlimb (~25°) and a steeply dipping forelimb (~75°), (2) an elliptical shape with nearly parallel limbs, consistent with a deep thrust fault beneath the subdome, (3) multiple thrust faults aligned parallel to the major axis, and (4) the vergence of both antiform and the exposed thrust faults are kinematically consistent. These characteristics align with the fault propagation folding model, where rocks bend in front of propagating thrust faults (Suppe and Medwedeff 1990; Fig. 11b). The steep forelimb and narrow interlimb angle (<85°) further support this model, as opposed to fault bend folding, which typically produces broad, flat-topped folds (Suppe 1983). These observations, coupled with the absence of signs of diapirism, or upwelling related to crustal extension, strongly favored the fault-propagation folding as the proper mechanism.

5.4.3 Abu Ziran synform

This synform is interpreted as hangingwall structure situated between the Um Baanib and Um Esh El-Hamra subdomes. Its geometry is shaped by the forelimb of the antiformal stack linked to the Um Baanib subdome and the back-limb of the Um Esh El-Hamra subdome. Numerous thrust faults, primarily dipping NE, traverse the fold and are interpreted as out-of-the-syncline thrusts, formed to accommodate the tightening of the fold (Butler, 1982). The extensive area of the synform and the shallow dip of its limbs support its classification as a hangingwall synform within a propagating thrust system.

5.4.4 Extensional fault-related antiform-synform pairs

Meatiq dome encompasses several antiform-synform pairs that spatially coexisted with extensional faults such as the Abu-Zohleiqa synform. The geometry and extent of the synform are controlled mainly by the neighboring NW-SE-trending normal fault. The fold is interpreted as a breached extensional fault-propagation fold developed by the succeeding propagation of normal fault through the highly foliated rocks of the Meatiq Succession (Fig. 11c). These structures are non-orogenic in origin, primarily associated with younger extensional faults, and likely formed during the Red Sea opening (~ 23 Ma; Bosworth et al., 2015).

5.4.4 Time constraints on the doming processes

The gneiss domes formed during the D_3 phase, driven by thrusting and folding associated with E-W oblique convergence (Fig. 12). This phase succeeded regional NW-directed tectonic transport and preceded the emplacement of post-tectonic plutons. Shearing in the Meatiq Dome has been

dated to >609 Ma, based on the emplacement of the Abu Ziran pluton (Andresen et al., 2009). Observations from the Um Baanib pluton extend the maximum shearing age to >631 Ma. Mild deformation in the Abu Ziran pluton (Mohammad and El Kazzaz, 2022) suggests its emplacement marked the cessation of shearing, further constraining the timeline to 605–600 Ma. Post-tectonic plutons (596–591 Ma) mark the end of orogenic processes, including doming, constraining the formation of the Meatiq Dome, and similar domes in CED at ~605–596 Ma.

6. Conclusions

This study presents several key findings regarding the Meatiq dome's nature, geometry, and evolution, leading to a revised model for the dome's development. The main findings are as follows:

1) Meatiq dome represents a domed thrust shear zone initiated at mid-crustal depths with sub-horizontal orientation. It developed primarily in quartz-rich metasediments, overlain by ophiolitic-island arc nappes. Microstructural analysis reveals crystal-plastic deformation, with varying strain across different lithologies, occurring at high to medium temperatures (~630–450°C). The prevailing shear sense is top-to-NW, indicating NW-directed tectonic transport.

2) The emplacement and crystallization of the Um Baanib granite were syn-kinematic, occurring concurrently with NW-directed regional shearing, as evidenced by microstructural transitions from magmatic to solid-state deformation, reflecting the dynamic interplay between pluton evolution and tectonic activity.

3) Both Um Baanib and Abu Ziran plutons have tabular geometries and were emplaced syn-kinematically along MSZ. Both plutons are dissected by thrust faults, emphasizing the dominance of brittle deformation during doming processes. The amphibolite bodies in the Um Baanib pluton are interpreted as sheets exposed along thrust faults.

4) Despite some similarities with MCCs, the absence of low-angle normal faults and evidence of regional extension argue against classifying the Meatiq Dome as an MCC. The dome's structure reflects a multi-phase deformation history controlled by NW-directed tectonic transport, followed by thrusting and folding.

5) The dome's geometry is primarily attributed to thrust-related folding, involving mechanisms such as antiformal stacking and fault-propagation folding. Its formation is tied to the D_3 phase, and subsequent extensional phases.

7. References

Abd El-Wahed, M. A. (2008). Thrusting and transpressional shearing in the Pan-African nappe southwest El-Sibai core complex, Central Eastern Desert, Egypt. *Journal of African Earth Sciences*, *50*(1), 16-36.

Abd El-Wahed, M. A. (2010). The role of the Najd Fault System in the tectonic evolution of the Hammamat molasse sediments, Eastern Desert, Egypt. Arabian Journal of Geosciences, 3, 1-26.

Abd El-Wahed, M. A. (2014). Oppositely dipping thrusts and transpressional imbricate zone in the Central Eastern Desert of Egypt. *Journal of African Earth Sciences*, *100*, 42-59.

Abd El-Wahed, M., & Attia, M. (2022). Genesis of the gneissic core complexes in the Arabian-Nubian Shield and its tectonic implications: A regional overview. Journal of Asian Earth Sciences, 236, 105337.

Abdeen, M. M., & Greiling, R. O. (2005). A quantitative structural study of late Pan-African compressional deformation in the Central Eastern Desert (Egypt) during Gondwana assembly. *Gondwana Research*, *8*(4), 457-471.

Abdelsalam, M. G., & Stern, R. J. (1996). Sutures and shear zones in the Arabian-Nubian Shield. *Journal* of African Earth Sciences, 23(3), 289-310.

Abu Sharib, A. S. A. A., Maurice, A. E., Abd El-Rahman, Y. M., Sanislav, I. V., Schulz, B., & Bakhit, B. R. (2019). Neoproterozoic arc sedimentation, metamorphism, and collision: Evidence from the northern tip of the Arabian-Nubian Shield and implication for the terminal collision between East and West Gondwana. Gondwana Research, 66, 13-42.

Abuzied, H.T. (1984). Geology of the Wadi Hamrawin area, Red Sea Hills, Eastern Desert, Egypt [Ph.D. thesis]: Columbia, University of South Carolina, 206 p.

Agar, R. A. (1987). The Najd fault system revisited; a two-way strike-slip orogen in the Saudi Arabian Shield. *Journal of Structural Geology*, *9*(1), 41-48.

Ali, K., Andresen, A., Manton, W. I., Stern, R. J., Omar, S. A., & Maurice, A. E. (2012). U–Pb zircon dating and Sr–Nd–Hf isotopic evidence to support a juvenile origin of the~ 634 Ma El Shalul granitic gneiss dome, Arabian–Nubian Shield. Geological Magazine, 149(5), 783-797.

Andresen, A., Augland, L. E., Boghdady, G. Y., Lundmark, A. M., Elnady, O. M., Hassan, M. A., & El-Rus, M. A. (2010). Structural constraints on the evolution of the Meatiq gneiss dome (Egypt), east-African orogen. *Journal of African Earth Sciences*, *57*(5), 413-422.

Andresen, A., El-Rus, M. A. A., Myhre, P. I., Boghdady, G. Y., & Corfu, F. (2009). U–Pb TIMS age constraints on the evolution of the Neoproterozoic Meatiq Gneiss dome, Eastern Desert, Egypt. *International Journal of Earth Sciences*, *98*, 481-497.

Be'eri-Shlevin, Y., Eyal, M., Eyal, Y., Whitehouse, M. J., & Litvinovsky, B. (2012). The Sa'al volcano-sedimentary complex (Sinai, Egypt): a latest Mesoproterozoic volcanic arc in the northern Arabian Nubian Shield. *Geology*, *40*(5), 403-406.

Bennett, J., Mosely, P. (1987). Tiered-tectonics and evolution, Eastern Desert and Sinai, Egypt. Current research in Africa Earth Science, Balkema, Rotterdam, The Netherlands, 79-82.

Blasband, B., White, S., Brooijmans, P., De Boorder, H., & Visser, W. (2000). Late Proterozoic extensional collapse in the Arabian–Nubian shield. *Journal of the Geological Society*, *157*(3), 615-628.

Bosworth, W., Stockli, D. F., & Helgeson, D. E. (2015). Integrated outcrop, 3D seismic, and geochronologic interpretation of Red Sea dike-related deformation in the Western Desert, Egypt–the role of the 23 Ma Cairo "mini-plume". *Journal of African Earth Sciences*, *109*, 107-119.

Boyer, S. E., & Elliott, D. (1982). Thrust systems. *AAPG bulletin*, *66*(9), 1196-1230.

Buck, W. R. (1988). Flexural rotation of normal faults. *Tectonics*, *7*(5), 959-973.

Butler, R. W. (1982). The terminology of structures in thrust belts. *Journal of structural Geology*, *4*(3), 239-245.

Cao, S., & Neubauer, F. (2016). Deep crustal expressions of exhumed strike-slip fault systems: Shear zone initiation on rheological boundaries. *Earth-Science Reviews*, *162*, 155-176.

Coney, P. J. (1980). Cordilleran metamorphic core complexes: An overview. *Geological Society of America Memoirs*, *153*, 7-31.

Deshesh, F. (2013). Metamorphic and Tectonic Studies of the Basement Rocks of Meatiq Area, Central Eastern Desert, Egypt. Master's thesis. Mansoura University, Egypt.

El Kalioubi, B., Fowler, AR., Abdelmalik, K. (2020). The Metamorphism and Deformation of the Basement Complex in Egypt. In: Hamimi, Z., El-Barkooky, A., Martínez Frías, J., Fritz, H., Abd El-Rahman, Y. (eds) The Geology of Egypt. Regional Geology Reviews. Springer, Cham. https://doi.org/10.1007/978-3-030-15265-9_6

El Kazzaz, Y. A. (2009). Kinematic indicators and sense of Hafafit Shear Zone: evidence and implication for pre-Pan-African Orogeny. Al Azhar Bulletin of Science, 20(1), 23-51.

El Kazzaz, Y. A. (2012). Thrust fault-related folds in El Hudi area, east Aswan city, South Eastern Desert, Egypt. Egyptian Journal of Geology, v. 56, 2012, p. 49-65.

El Ramly, M. F., Greiling, R. O., & Rashwan, A. A. (1990). Comment on "Extension of the Najd Shear System from Saudi Arabia to the Central Eastern Desert of Egypt based on integrated field and LANDSAT observations" by M. Sultan, RE Arvidson, IJ Duncan, RJ Stern, and B. El Kaliouby. Tectonics, 9(3), 535-538.

El-Bialy, M.Z. (2020). Precambrian Basement Complex of Egypt. In: Hamimi, Z., El-Barkooky, A., Martínez Frías, J., Fritz, H., Abd El-Rahman, Y. (eds) The Geology of Egypt. Regional Geology Reviews. Springer, Cham. https://doi.org/10.1007/978-3-030-15265-9_2

El-Gaby, S., El-Nady, O., & Khudeir, A. (1984). Tectonic evolution of the basement complex in the Central Eastern Desert of Egypt. *Geologische Rundschau*, *73*, 1019-1036.

Eskola, P.E. (1949), The problem of mantled gneiss domes: Geological Society of London, Quarterly Journal, v. 104, p. 461–476.

Farahat, E. S. (2010). Neoproterozoic arc–back-arc system in the Central Eastern Desert of Egypt: evidence from supra-subduction zone ophiolites. *Lithos*, *120*(3-4), 293-308.

Forster, M. A., & Lister, G. S. (1999). Detachment faults in the Aegean core complex of Ios, Cyclades, Greece. *Geological Society, London, Special Publications*, *154*(1), 305-323.

Fowler, A. R., & El Kalioubi, B. (2002). The Migif–Hafafit gneissic complex of the Egyptian Eastern Desert: fold interference patterns involving multiply deformed sheath folds. Tectonophysics, 346(3-4), 247-275.

Fowler, A. R., & El Kalioubi, B. (2004). Gravitational collapse origin of shear zones, foliations and linear structures in the Neoproterozoic cover nappes, Eastern Desert, Egypt. Journal of African Earth Sciences, 38(1), 23-40.

Fowler, A. R., Khamees, H., & Dowidar, H. (2007). El Sibai gneissic complex, Central Eastern Desert, Egypt: folded nappes and syn-kinematic gneissic granitoid sheets–not a core complex. Journal of African Earth Sciences, 49(4-5), 119-135.

Fowler, A., & Osman, A. F. (2013). Sedimentation and inversion history of three molasse basins of the western Central Eastern Desert of Egypt: implications for the tectonic significance of Hammamat basins. *Gondwana Research*, *23*(4), 1511-1534.

Fowler, A., Hassen, I. S., & Hassan, M. (2018). The Feiran-Solaf metamorphic complex, Sinai, Egypt: Evidence for orthogonal or oblique tectonic convergence? *Journal of African Earth Sciences*, *146*, 48-65.

Fowler, AR., Hamimi, Z. (2020). Structural and Tectonic Framework of Neoproterozoic Basement of Egypt: From Gneiss Domes to Transpression Belts. In: Hamimi, Z., El-Barkooky, A., Martínez Frías, J., Fritz, H., Abd El-Rahman, Y. (eds) The Geology of Egypt. Regional Geology Reviews. Springer, Cham. https://doi.org/10.1007/978-3-030-15265-9_3

Fowler, AR., Hamimi, Z. (2021). Post-amalgamation Depositional Basins in the Arabian-Nubian Shield: The Hammamat Basins of Egypt. In: Hamimi, Z., Fowler, AR., Liégeois, JP., Collins, A., Abdelsalam, M.G., Abd EI-Wahed, M. (eds) The Geology of the Arabian-Nubian Shield. Regional Geology Reviews. Springer, Cham. https://doi.org/10.1007/978-3-030-72995-0_19

Fowler, T. J., & Osman, A. F. (2001). Gneiss-cored interference dome associated with two phases of late Pan-African thrusting in the central Eastern Desert, Egypt. Precambrian Research, 108(1-2), 17-43.

878 Fritz, H., Dallmeyer, D. R., Wallbrecher, E., Loizenbauer, J., Hoinkes, G., Neumayr, P., & Khudeir, A. A. (2002).
879 Neoproterozoic tectonothermal evolution of the Central Eastern Desert, Egypt: a slow velocity tectonic process of
880 core complex exhumation. Journal of African Earth Sciences, 34(3-4), 137-155.

881 Fritz, H., Wallbrecher, E., Khudeir, A. A., El Ela, F. A., & Dallmeyer, D. R. (1996). Formation of Neoproterozoic
882 metamorphic complex during oblique convergence (Eastern Desert, Egypt). Journal of African Earth Sciences, 23(3),
883 311-329.

884 Gamal El Dien, H., Hamdy, M., El-Ela, A. S. A., Abu-Alam, T., Hassan, A., Kil, Y., Mizukami, T.& Soda, Y. (2016).
885 Neoproterozoic serpentinites from the Eastern Desert of Egypt: insights into Neoproterozoic mantle geodynamics and
886 processes beneath the Arabian-Nubian Shield. *Precambrian Research*, *286*, 213-233.

887 Genna, A., Nehlig, P., Le Goff, E., Guerrot, C., & Shanti, M. J. P. R. (2002). Proterozoic tectonism of the Arabian
888 Shield. *Precambrian Research*, *117*(1-2), 21-40.

889 Godin, L., Grujic, D., Law, R. D., & Searle, M. P. (2006). Channel flow, ductile extrusion and exhumation in
890 continental collision zones: an introduction. *Geological Society, London, Special Publications*, *268*(1), 1-23.

891 Greiling, R. O. (1997). Thrust tectonics in crystalline domains: the origin of a gneiss dome. *Proceedings of the Indian*
892 *Academy of Sciences-Earth and Planetary Sciences*, *106*, 209-220.

893 Greiling, R. O., Abdeen, M. M., Dardir, A. A., El Akhal, H., El Ramly, M. F., El Din Kamal, G. M., G.M., Osman,
894 A.F., Rashwan, A.A., Rice, A.H.N. & Sadek, M. F. (1994). A structural synthesis of the Proterozoic Arabian-Nubian
895 Shield in Egypt. Geologische Rundschau, 83, 484-501.

896 Habib, M. E., Ahmed, A. A., & El Nady, O. M. (1985a). Two orogenies in the Meatiq area of the Central Eastern
897 Desert, Egypt. *Precambrian Research*, *30*(2), 83-111.

898 Habib, M. E., Ahmed, A. A., & El Nady, O. M. (1985b). Tectonic evolution of the Meatiq infrastructure, central
899 Eastern Desert, Egypt. *Tectonics*, *4*(7), 613-627.

900 Hamdy, M. M., Abd El-Wahed, M. A., El Dien, H. G., & Morishita, T. (2017). Garnet hornblendite in the Meatiq
901 Core Complex, Central Eastern Desert of Egypt: implications for crustal thickening preceding the~ 600 Ma
902 extensional regime in the Arabian-Nubian Shield. *Precambrian Research*, *298*, 593-614.

903 Hamimi, Z., Fowler, AR. (2021). Najd Shear System in the Arabian-Nubian Shield. In: Hamimi, Z., Fowler, AR.,
904 Liégeois, JP., Collins, A., Abdelsalam, M.G., Abd EI-Wahed, M. (eds) The Geology of the Arabian-Nubian Shield.
905 Regional Geology Reviews. Springer, Cham. https://doi.org/10.1007/978-3-030-72995-0_15

906 Hassan, M., Abu-Alam, T. S., Stüwe, K., Fowler, A., & Hassen, I. (2014). Metamorphic evolution of the Sa'al–Zaghra
907 Complex in Sinai: Evidence for Mesoproterozoic Rodinia break-up?. *Precambrian Research*, *241*, 104-128.

908 Hassan, M., Abu-Alam, T., Fowler, AR. (2021). The Sinai Metamorphic Complexes from Rodinia Rifting to the
909 Gondwana Collision. In: Hamimi, Z., Arai, S., Fowler, AR., El-Bialy, M.Z. (eds) The Geology of the Egyptian Nubian
910 Shield. Regional Geology Reviews. Springer, Cham. https://doi.org/10.1007/978-3-030-49771-2_4

911 Hassan, M., Stüwe, K., Abu-Alam, T. S., Klötzli, U., & Tiepolo, M. (2016). Time constraints on deformation of the
912 Ajjaj branch of one of the largest Proterozoic shear zones on Earth: The Najd Fault System. Gondwana Research, 34,
913 346-362.

914 Hassan, S. M., El Kazzaz Y., Taha, M. M. & Mohammad, A. T. (2017). Late Neoproterozoic basement rocks of
915 Meatiq area, Central Eastern Desert, Egypt: petrography and remote sensing characterizations. *Journal of African*
916 *Earth Sciences*, *131*, 14-31.

917 Heaverlo, N. D. (2014). Stress and strain rate estimates associated with penetrative deformation of the Harkless
918 quartzite aureole rocks, Papoose Flat Pluton, California/Using structure contour maps to analyze subsurface 3D fault
919 geometry along segments of the Moine Thrust (Doctoral dissertation, Virginia Tech).

Hirth, G., & Tullis, J. A. N. (1992). Dislocation creep regimes in quartz aggregates. *Journal of structural geology*, *14*(2), 145-159.

Hunter, N. J., Hasalová, P., Weinberg, R. F., & Wilson, C. J. (2016). Fabric controls on strain accommodation in naturally deformed mylonites: The influence of interconnected micaceous layers. *Journal of Structural Geology*, 83, 180-193.

Hunter, N. J., Weinberg, R. F., Wilson, C. J., Luzin, V., & Misra, S. (2018). Microscopic anatomy of a "hot-on-cold" shear zone: Insights from quartzites of the Main Central Thrust in the Alaknanda region (Garhwal Himalaya). GSA Bulletin, 130(9-10), 1519-1539.

Hutton, D.H., 1992. Granite sheeted complexes: evidence for the dyking ascent mechanism. Earth Environ. Sci. Trans. R. Soc. Edinb. 83 (1–2), 377–382. https://doi.org/10.1017/S0263593300008038.

Hutton, D.H., 1996. The space problem in the emplacement of granite. Episodes J. Int. Geosci. 19 (4), 114–119. https://doi.org/10.18814/epiiugs/1996/v19i4/004.

Hutton, D.H.W., Dempster, T.J., Brown, P.E., Becker, S.D., 1990. A new mechanism of granite emplacement: intrusion in active extensional shear zones. Nature 343 (6257), 452–455. https://doi.org/10.1038/343452a0.

Jarrar, G., Baumann, A., & Wachendorf, H. (1983). Age-determinations In the Precambrian Basement of the Wadi Araba area, SW Jordan. in Fortschritte der Mineralogie (vol. 61, no. 1, pp. 102-102). Naegele u Obermiller Johannesstrasse 3a, d 70176 Stuttgart, Germany: E Schweizerbart'sche Verlags.

Jarrar, G., Saffarini, G., Baumann, A., & Wachendorf, H. (2004). Origin, age and petrogenesis of Neoproterozoic composite dikes from the Arabian-Nubian Shield, SW Jordan. Geological Journal, 39(2), 157-178.

Jessup, M. J., Langille, J. M., Diedesch, T. F., & Cottle, J. M. (2019). Gneiss dome formation in the Himalaya and southern Tibet. *Geological Society, London, Special Publications*, *483*(1), 401-422.

Johnson, P. R., Andresen, A., Collins, A. S., Fowler, A. R., Fritz, H., Ghebreab, W., Kusky, T. & Stern, R. J. (2011). Late Cryogenian–Ediacaran history of the Arabian–Nubian Shield: a review of depositional, plutonic, structural, and tectonic events in the closing stages of the northern East African Orogen. *Journal of African Earth Sciences*, *61*(3), 167-232.

Law, R. D. (2014). Deformation thermometry based on quartz c-axis fabrics and recrystallization microstructures: A review. *Journal of structural Geology*, *66*, 129-161.

Law, R. D., Morgan, S. S., Casey, M., Sylvester, A. G., & Nyman, M. (1992). The Papoose Flat Pluton of eastern California: a reassessment of its emplacement history in the light of new microstructural and crystallographic fabric observations. Earth and Environmental Science Transactions of the Royal Society of Edinburgh, 83(1-2), 361-375.

Lister, G. S., & Davis, G. A. (1989). The origin of metamorphic core complexes and detachment faults formed during Tertiary continental extension in the northern Colorado River region, USA. *Journal of Structural Geology*, *11*(1-2), 65-94.

Loizenbauer, J., Wallbrecher, E., Fritz, H., Neumayr, P., Khudeir, A. A., & Kloetzli, U. (2001). Structural geology, single zircon ages and fluid inclusion studies of the Meatiq metamorphic core complex: implications for Neoproterozoic tectonics in the Eastern Desert of Egypt. Precambrian Research, 110(1-4), 357-383.

Lundmark, A. M., Andresen, A., Hassan, M. A., Augland, L. E., & Boghdady, G. Y. (2012). Repeated magmatic pulses in the East African Orogen in the Eastern Desert, Egypt: an old idea supported by new evidence. *Gondwana Research*, *22*(1), 227-237.

Makroum, F. (2017). Structural interpretation of the Wadi Hafafit culmination: a Pan-African gneissic dome in the central Eastern Desert, Egypt. *Lithosphere*, *9*(5), 759-773.

Mancktelow, N. S., & Pavlis, T. L. (1994). Fold-fault relationships in low-angle detachment systems. *Tectonics*, *13*(3), 668-685.

McClay, K. R. (1992). Glossary of thrust tectonics terms. *Thrust tectonics*, 419-433.

Meert, J. G. (2003). A synopsis of events related to the assembly of eastern Gondwana. *Tectonophysics*, *362*(1-4), 1-40.

Meyer, S. E., Passchier, C., Abu-Alam, T., & Stüwe, K. (2014). A strike-slip core complex from the Najd fault system, Arabian shield. *Terra Nova*, *26*(5), 387-394.

Mitra, G., Bhattacharyya, K., & Mukul, M. (2010). The Lesser Himalayan duplex in Sikkim: Implications for variations in Himalayan shortening. *Journal of the Geological Society of India*, *75*, 289-301.

Moghazi, A. M., Hassanen, M. A., & Mohamed, F. H. (1997). Source and evolution history of some Mesozoic alkaline volcanics in the Eastern Desert of Egypt: inference from petrology and geochemistry. Journal of African Earth Sciences, 24(1-2), 11-28.

Mohammad, A. T., & El Kazzaz, Y. A. (2022). Geometry and growth of syn-tectonic plutons emplaced in thrust shear zones: Insights from Abu Ziran pluton, Egypt. *Journal of Structural Geology*, *162*, 104689.

Mohammad, A. T., El Kazzaz, Y. A., Hassan, S. M., & Taha, M. M. (2020). Neoproterozoic tectonic evolution and exhumation history of transpressional shear zones in the East African orogen: implications from kinematic analysis of Meatiq area, Central Eastern Desert of Egypt. International Journal of Earth Sciences, 109, 253-279.

Morgan, S. S., & Law, R. D. (1998). Concordant plutons and two periods of porphyroblast growth: Products of multiple magma injection. Pluton Emplacement, Aureole Deformation and Metamorphism, and Regional Deformation Within the Central White-Inyo Range, Eastern California, 155.

Mostafa, A., El-Barkooky, A., & Hammed, M. (2023). Structural geometry and tectonic evolution of an Early Cretaceous rift crossing the Nile Valley in Upper Egypt. *Marine and Petroleum Geology*, *153*, 106289.

Neumayr, P., Hoinkes, G., Puhl, J., Mogessie, A., & Khudeir, A. A. (1998). The Meatiq dome (Eastern Desert, Egypt) a Precambrian metamorphic core complex: petrological and geological evidence. *Journal of Metamorphic Geology*, *16*(2), 259-279.

Neumayr, P., Mogessie, A., Hoinkes, G., & Puhl, J. (1996). Geological setting of the Meatiq metamorphic core complex in the Eastern Desert of Egypt based on amphibolite geochemistry. *Journal of African Earth Sciences*, *23*(3), 331-345.

Nyman, M. W., Law, R. D., & Morgan, S. S. (1995). Conditions of contact metamorphism, Papoose Flat Pluton, eastern California, USA: implications for cooling and strain histories. Journal of Metamorphic Geology, 13(5), 627-643.

Omar, G. I., & Steckler, M. S. (1995). Fission track evidence on the initial rifting of the Red Sea: two pulses, no propagation. *Science*, *270*(5240), 1341-1344.

Passchier, C. W., & Trouw, R. A. (2005). *Microtectonics*. Springer Science & Business Media.

Paterson, S. R., Vernon, R. H., & Tobisch, O. T. (1989). A review of criteria for the identification of magmatic and tectonic foliations in granitoids. *Journal of structural geology*, *11*(3), 349-363.

Petford, N., Cruden, A.R., McCaffrey, K.J.W., Vigneresse, J.L., 2000. Granite magma formation, transport and emplacement in the Earth's crust. Nature 408 (6813), 669–673. https://doi.org/10.1038/35047000.

Platt, J. P., Behr, W. M., & Cooper, F. J. (2015). Metamorphic core complexes: Windows into the mechanics and rheology of the crust. *Journal of the Geological Society*, *172*(1), 9-27.

Ries, A. C., Shackleton, R. M., Graham, R. H., & Fitches, W. R. (1983). Pan-African structures, ophiolites and mélange in the Eastem Desert of Egypt: a traverse at 26 N. *Journal of the Geological Society*, *140*(1), 75-95.

Schürmann, H. M. E. (1966). The pre-cambrian along the guld of suez and the norther part of the red sea. Brill Archive.

Shalaby, A. (2010). The northern dome of Wadi Hafafit culmination, Eastern Desert, Egypt: structural setting in tectonic framework of a scissor-like wrench corridor. Journal of African Earth Sciences, 57(3), 227-241.

Shalaby, A., Stüwe, K., Makroum, F., Fritz, H., Kebede, T., & Klötzli, U. (2005). The Wadi Mubarak belt, Eastern Desert of Egypt: a Neoproterozoic conjugate shear system in the Arabian–Nubian Shield. *Precambrian Research*, *136*(1), 27-50.

Shoorangiz, M., Sarkarinejad, K., & Dehsarvi, L. H. (2019). Structural characteristic of a thrust system related gneiss dome of the Zagros hinterland-fold-and-thrust belt: The Sourian and Tutak metamorphic complexes, SW Iran. *Journal of African Earth Sciences*, *151*, 337-350.

Steckler, M. S., & Omar, G. I. (1994). Controls on erosional retreat of the uplifted rift flanks at the Gulf of Suez and northern Red Sea. *Journal of Geophysical Research: Solid Earth*, *99*(B6), 12159-12173.

Stern, R. J. (1994). Arc assembly and continental collision in the Neoproterozoic African Orogen: implications for the consolidation of Gondwanaland. Annual Review Of Earth And Planetary Sciences, Volume 22, pp. 319-351., 22, 319-351.

Stern, R. J. (2018). Neoproterozoic formation and evolution of Eastern Desert continental crust–The importance of the infrastructure-superstructure transition. *Journal of African Earth Sciences*, *146*, 15-27.

Stern, R. J., Gottfried, D., & Hedge, C. E. (1984). Late Precambrian rifting and crustal evolution in the Northeastern Desert of Egypt. Geology, 12(3), 168-172.

Stipp, M., Stünitz, H., Heilbronner, R., & Schmid, S. M. (2002a). The eastern Tonale fault zone: a 'natural laboratory for crystal plastic deformation of quartz over a temperature range from 250 to 700 C. *Journal of structural geology*, *24*(12), 1861-1884.

Stipp, M., Stünitz, H., Heilbronner, R., & Schmid, S. M. (2002b). Dynamic recrystallization of quartz: correlation between natural and experimental conditions. *Geological Society, London, Special Publications*, *200*(1), 171-190.

Sturchio, N. C., Sultan, M., & Batiza, R. (1983). Geology and origin of Meatiq Dome, Egypt: a Precambrian metamorphic core complex?. Geology, 11(2), 72-76.

Sultan, M., Arvidson, R. E., Duncan, I. J., Stern, R. J., & El Kaliouby, B. (1988). Extension of the Najd shear system from Saudi Arabia to the central Eastern Desert of Egypt based on integrated field and Landsat observations. Tectonics, 7(6), 1291-1306.

Suppe, J. (1983). Geometry and kinematics of fault-bend folding. *American Journal of science*, *283*(7), 684-721.

Suppe, J., & Medwedeff, D. A. (1990). Geometry and kinematics of fault-propagation folding. *Eclogae Geologicae Helvetiae*, *83*(3), 409-454.

Surour, A. A., Madani, A. A., & El-Sharkawi, M. A. (2024). Mineralogical and geochemical characterization of the Wadi Natash volcanic field (WNVF), Egypt: Alkaline magmatism in a Late Cretaceous continental rift system. Acta Geochimica, 1-23.

Teyssier, C., & Whitney, D. L. (2002). Gneiss domes and orogeny. *Geology*, *30*(12), 1139-1142.

Tullis, J. (1983). Deformation of feldspars. *Feldspar mineralogy*, *2*, 297-323.

Vernon, R. H. (2000). Review of microstructural evidence of magmatic and solid-state flow. *Visual Geosciences*, *5*, 1-23.

Wawrzyniec, T. F., Selverstone, J., & Axen, G. J. (2001). Styles of footwall uplift along the Simplon and Brenner normal fault systems, central and Eastern Alps. *Tectonics*, *20*(5), 748-770.

Wernicke, B. (1995). Low-angle normal faults and seismicity: A review. *Journal of Geophysical Research: Solid Earth*, *100*(B10), 20159-20174.

Whitney, D.L, Teyssier, C., and Vanderhaeghe, O. (2004). Gneiss domes and crustal fl ow, in Whitney, D.L, Teyssier, C., and Siddoway, C.S., Gneiss domes in orogeny: Boulder, Colorado, Geological Society of America Special Paper 380, p. 15–33.

Yin, A., 2004, Gneiss domes and gneiss dome systems, in Whitney, D.L., Teyssier, C., and Siddoway, C.S., eds., Gneiss domes in orogeny: Boulder, Colorado, Geological Society of America Special Paper 380, p. 1–14.

Zibra, I., Kruhl, J. H., Montanini, A., & Tribuzio, R. (2012). Shearing of magma along a high-grade shear zone: Evolution of microstructures during the transition from magmatic to solid-state flow. *Journal of Structural Geology*, *37*, 150-160.

Figure captions

Fig. 1 (a) Simplified geological map for the Central Eastern Desert (CED) of Egypt (after Johnson et al., 2011), (b) Map showing the distribution of the metamorphic complexes in the CED. (Abbreviations: NED = North Eastern Desert, HSZ= Hamrawin Shear Zone, EMSZ= East Meatiq Shear zone, ASZ= Atalla Shear Zone).

Fig. 2 Geological map of Meatiq dome illustrating the main rock units and geological structures. The stereograms indicate the field measurements of tectonic foliation and lineations collected from rocks in the Meatiq Dome.

Fig. 3 Brittle thrusts and normal faults in Meatiq Succession. (a) Repetition of rock units along the eastern flank of the dome, caused by multiple thrusting events. (b) Field photograph perpendicular to the thrust strike, highlighting the distinctive wedge-shaped thrust sheets within a duplex structure, and the structural intercalation of hornblende schist with quartzo-feldspathic schist. (c) Thrust faults in the Um Baanib granite and along its boundaries with amphibolites. (d) Close-up view of thrust fault surface in the granite, marked by white inset in the previous image, revealing a closely-spaced network of anastomosing thrust slices and faults. (e-f) Thrust duplex structure within the Um Baanib granite on the northern flank of the dome. (g) Thrust duplex structure cutting across the Abu Ziran pluton. (a) Steep normal faults intersect the Um Baanib Pluton along the northern flank of the dome and show distinct cross-cutting relationships with earlier low-angle thrust faults.

Fig. 4 Series of geological cross sections constructed in various orientations across the Meatiq Dome. All interpretations are based on detailed structural observations and analyses.

Fig. 5 Structural characteristics of the Meatiq Succession. (a) Tectonic penetrative foliation observed in mica-rich schist and phyllonites. (b) Granite sheets and intrusions were placed parallel to the foliation within quartzo-feldspathic schist. (c) Schematic illustration of transposed foliation with rootless intrafolial folds in the sheared rocks of the Abu Fannani thrust sheet. (d) Polished hand specimen sectioned perpendicular to the stretching lineation, with a tracing of key structures showing transposed foliation, boudinaged layering, and intrafolial folds. (e) Well-developed stretched mineral lineation in deformed granite from Um Baanib. (f) Stretched mineral lineation in schist, defined by elongated garnet crystals. (g) Pinch-and-swell structure in a quartz vein. (h) Boudinaged and highly sheared quartz veins in mylonites. (i) Sigmoidal asymmetric boudin of intrusive rock within highly sheared rocks, indicating top-to-NW shearing. (j) Sigmoidal asymmetric boudin of quartz within highly sheared rocks, also indicating top-to-NW shearing. (k) Foliation boudinage in quartzo-feldspathic schist, bounded by highly ductile mica-rich rocks.

Fig. 6 Mesoscopic Folds in the Meatiq Succession. (a) Outcrop-scale recumbent fold developed in mica-rich schist and mylonites along the southern flank of the dome. (b), (c) Overturned folds formed in sequences of competent and non-competent layers, featuring a distinctive hinge collapse structure at the crest due to flexural slip and the flow of incompetent layers. (d) Recumbent fold with rounded hinges in mica-rich schist and mylonites. (e) Tight intrafolial folds in sheared schist and mylonites. (f) Sheath fold with eye-shaped geometry, indicating significant simple shear deformation.

Fig. 7 Microstructure of Um Baanib deformed granite. The abbreviations are (qtz) for quartz, (kfs) for potassium feldspar, (pg) for plagioclase feldspar, (bt) for biotite, (GBM) for Grain Boundary Migration, and (CSZ) for Cataclastic Shear Zone. (a-d) Photomicrographs showing relicts of earlier magmatic shape-preferred orientation, characterized by euhedral to subhedral plagioclase crystals (crossed nicols, CN). (e) Well-aligned euhedral plagioclase crystals, oriented parallel to the main fabric, embedded within large K-feldspar crystals, exhibiting a distinctive poikilitic texture (CN). (f) Flame-shaped perthites in K-feldspar crystal (CN). (g) GBM recrystallization textures in plagioclase crystals with serrated crystal margins, indicative of solid-state deformation (CN). (h) GBM recrystallization in quartz is defined by highly serrated crystal margins (CN). (i) Elongated quartz crystals and ribbons with distinctive GBM, aligned parallel or subparallel to the main tectonic fabric defined by biotite laths (CN). (j) Undulatory extinction in quartz, indicating low-temperature

solid-state deformation (CN). (k-l) Cataclastic shear zone cutting across the earlier ductile fabric (CN).

Fig. 8 Simplified schematic diagram illustrating the different microstructures observed Meatiq Succession. (a) sketch geological map showing the eastern transect along the eastern flank of the dome with sample locations. (b) Lithologic log depicting the rock Succession along the eastern transect, dominant mineral phases, and corresponding microstructures observed in each unit. Deformation temperatures were estimated based on microstructural style variations and correlated with metamorphic conditions estimated by Neymayr et al. (1998), assuming coeval deformation and regional metamorphism. (c) Schematic diagram illustrating the main microstructures observed in different thrust sheets, highlighting variations in their styles and distributions.

Fig. 9 Photomicrographs illustrating the dominant microstructural styles observed in MSZ. The abbreviations are (qtz) for quartz, (kfs) for potassium feldspar, (pg) for plagioclase feldspar, (ms) for muscovite, (bt) for biotite, (sil) for sillimanite, (grt) for garnet, (GBM) for Grain Boundary Migration, (CBE) chessboard extinction. (a) Elongated quartz ribbons define grain-shaped foliation (CN). Note the alignment of mica fish and sillimanite fibers parallel to the foliation. (b-c) Quartz crystals with highly sutured and serrated boundaries, indicate GBM (CN). (d) White mica fish exhibiting well-developed sigmoidal shapes, suggesting an apparent sinistral (top-to-left) shear sense (CN). (e) Localized development of CBE in quartz crystals (CN). (f) Mylonitic foliation, defined by mica laths, wraps around augen structures of quartz aggregates in micaceous quartzite (CN). (g-h) Mica-rich varieties show poorly developed stretching and deformation of quartz grains, with most of the deformation accommodated by mica crystals and laths (CN). (i) Porphyroclast of plagioclase wrapped by mylonitic foliation, defined by biotite crystals, indicating an apparent sinistral (top-to-left) shear sense (CN). (j) Garnet porphyroblast preserving S-shaped foliation, defined by quartz inclusion trails, truncated against the penetrative differentiated foliation (S2), which wraps around the porphyroblast and is defined by quartz and muscovite (CN). (k) Shear bands (C') cutting across the mylonitic foliation, indicating a top-to-left shear sense (plain polarized light, PPL). (l) Tight intrafolial fold in a quartz vein, indicating an apparent dextral (top-to-right) shear sense (CN).

Fig. 10 Block Diagram summarizing our structural observations of the Meatiq Dome and illustrating its structural characteristics and overall architecture.

Fig. 11 Schematic diagrams illustrating the proposed structural mechanisms and processes responsible for the formation of the Meatiq Dome and its internal structures. (a) Antiformal stack model for the Um Baanib Subdome, (b) fault-propagation fold model for the Um Esh El-Hamra Subdome, and (c) extensional fault propagation folding, explaining the antiform-synform pairs associated with extensional faults

Fig. 12 Schematic diagrams depicting the structural evolution of the Meatiq Dome, including the various stages of folding and the final doming.

Supplementary materials

Supplementary 1 Structural Features of the Um Baanib and Um Esh El-Hamra Subdomes. (a) Moderately dipping quartzo-feldspathic schist and mylonites along the eastern flank of the Um Baanib subdome. (b) Southern limb of the Um Baanib subdome, exhibiting moderately dipping phyllonites and amphibolites. (c) Panoramic view of the Um Esh El-Hamra subdome, highlighting its distinctive asymmetric limb dipping. (d) Steeply dipping phyllonites and biotite schist along the western flank of the Um Esh El-Hamra subdome.

Supplementary 2 3D block diagrams showing interpreted structural cross-sections across (a) Um Esh El-Hamra Subdome, (b) Abu Zohleiq synform, and (c) Abu Ziran Synform. The interpretation is based on surface structural data.

Supplementary 3 Characteristics of sheet-shaped intrusions associated with the Um Baanib Pluton. (a-d) Various styles of tabular and sheet-shaped intrusions of Um Baanib granite were emplaced parallel to the ductile fabric in the Meatiq Succession. (e-f) Sheet-shaped intrusions of Um Baanib granite that intruded into amphibolites (at the core of the pluton), parallel to the foliation and ductile fabrics. (g-h) Schematic diagrams depicting the interpreted geometry and tectonic environment for the early emplacement of the Um Baanib Pluton during initial shearing, and the later emplacement of the tabular intrusion of Abu Ziran during advanced shearing.

Supplementary 4 Satellite images illustrating the main geometries and distribution of amphibolite sheets in the Meatiq Dome. (a) A tilted view of the Google Earth satellite image shows a major arcuate belt of amphibolites intersecting Um Baanib granite, which is bound by thrust faults. (b) Close-up view of the amphibolite belt along the eastern flank of the dome. (c) Google Earth image highlighting sheet-shaped amphibolites trending predominantly N-S and aligned with the thrust faults. (d) Satellite image depicting a major sheet-shaped body of amphibolite along the eastern flank of the dome. (e) and (f) Satellite images of sheet-shaped amphibolite bodies along the northern side of the dome. (g) A satellite image draped over a DEM to reveal the 3D shape of the amphibolite sheets and associated thrust faults. (h) The Map sketch shows the spatial distribution of the thrust sheets within the pluton and their relationship to the thrust faults intersecting it.

Figure

Click here to access/download;Figure;Figures_final_compressed.pdf

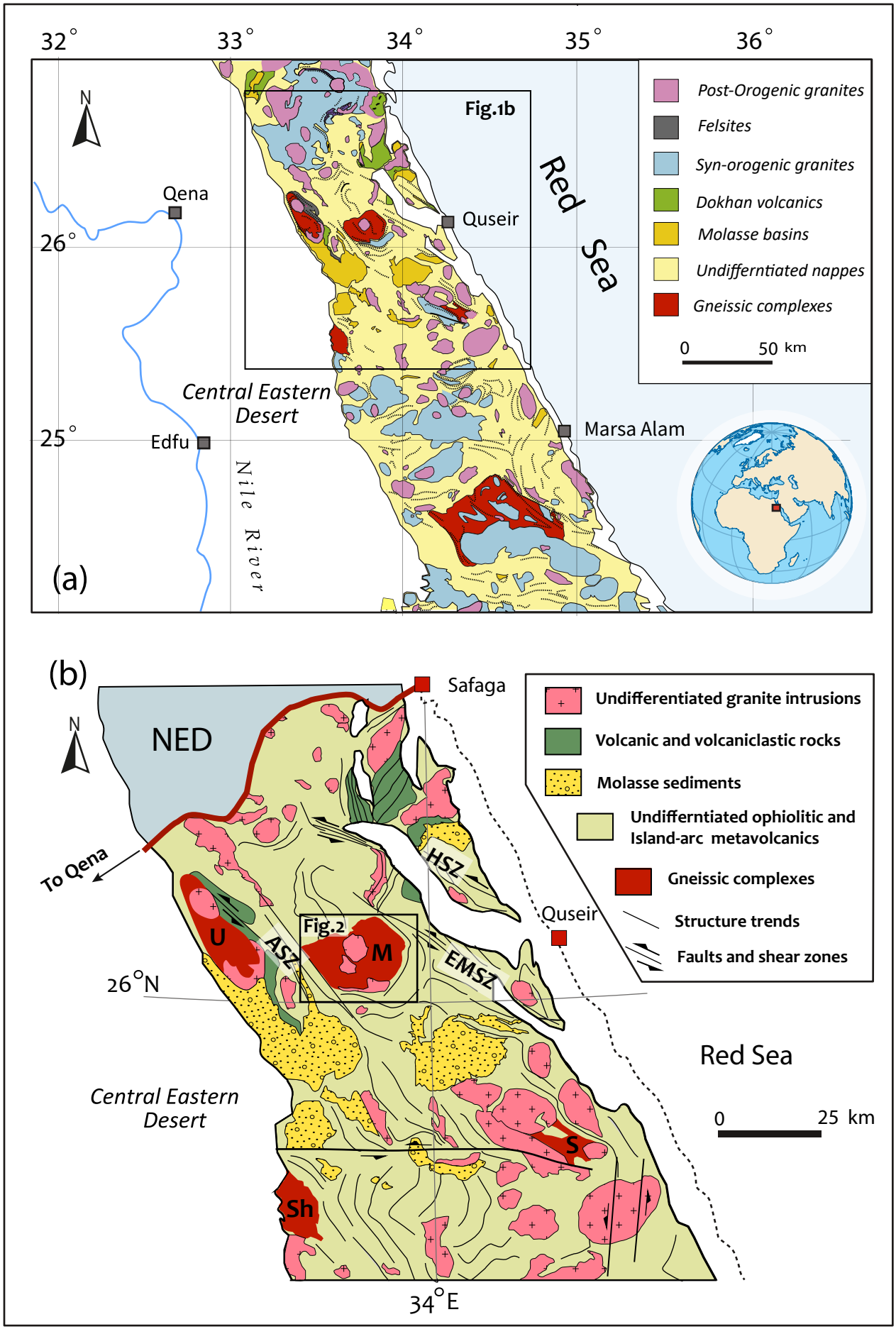

33°40'E
33°45'E
33°50'E
33°55'E
26°10'N
26°05'N
26°00'N
Sodemin fault
Um Baanib subdome
Abu Zohleiqa synform
Wadi Murr
Um Esh El Hamra subdome
Abu Ziran synform
Wadi Abu Ziran
Abu Ziran fault
N
0
4
8
Km

Legend

Structural symbols

- Normal faults
- Thrust faults
- Strike-slip faults
- Synform
- Antiform
- Subdome

Tectonostratigraphy

- Wadi deposits
- Granite Intrusions
  - Arieki granites
  - Abu Ziran granites
  - Um Baanib deformed granite
- Ophiolitic- Island arc Succession
  - Sheared molasse sediments
  - Sheared metavolcanics, and amphibolites
  - Massive basic and intermediate metavolcanics
  - Metagabbroes
  - Serpentinites and talc carbonates
- Meatiq Succession
  - Abu Fannani thrust sheet
  - Abu Zohleia thrust sheet
  - Um Esh El-Hamra thrust sheet

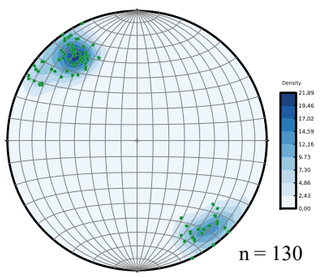

Mineral Stretching Lineation

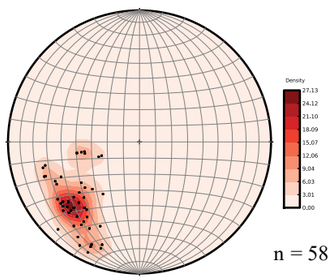

Foliation (Eastern flank)

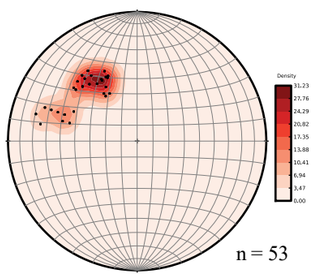

Foliation (Southern flank)

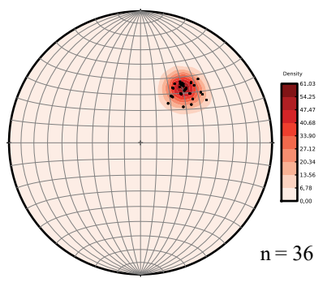

Foliation (Western flank)

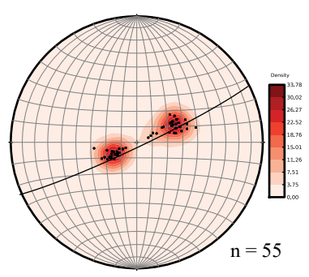

Foliation (W. Um Esh El-Hamra)

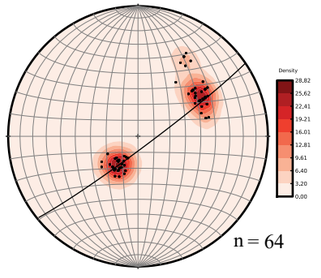

Foliation (W. Abu Zohleiqa)

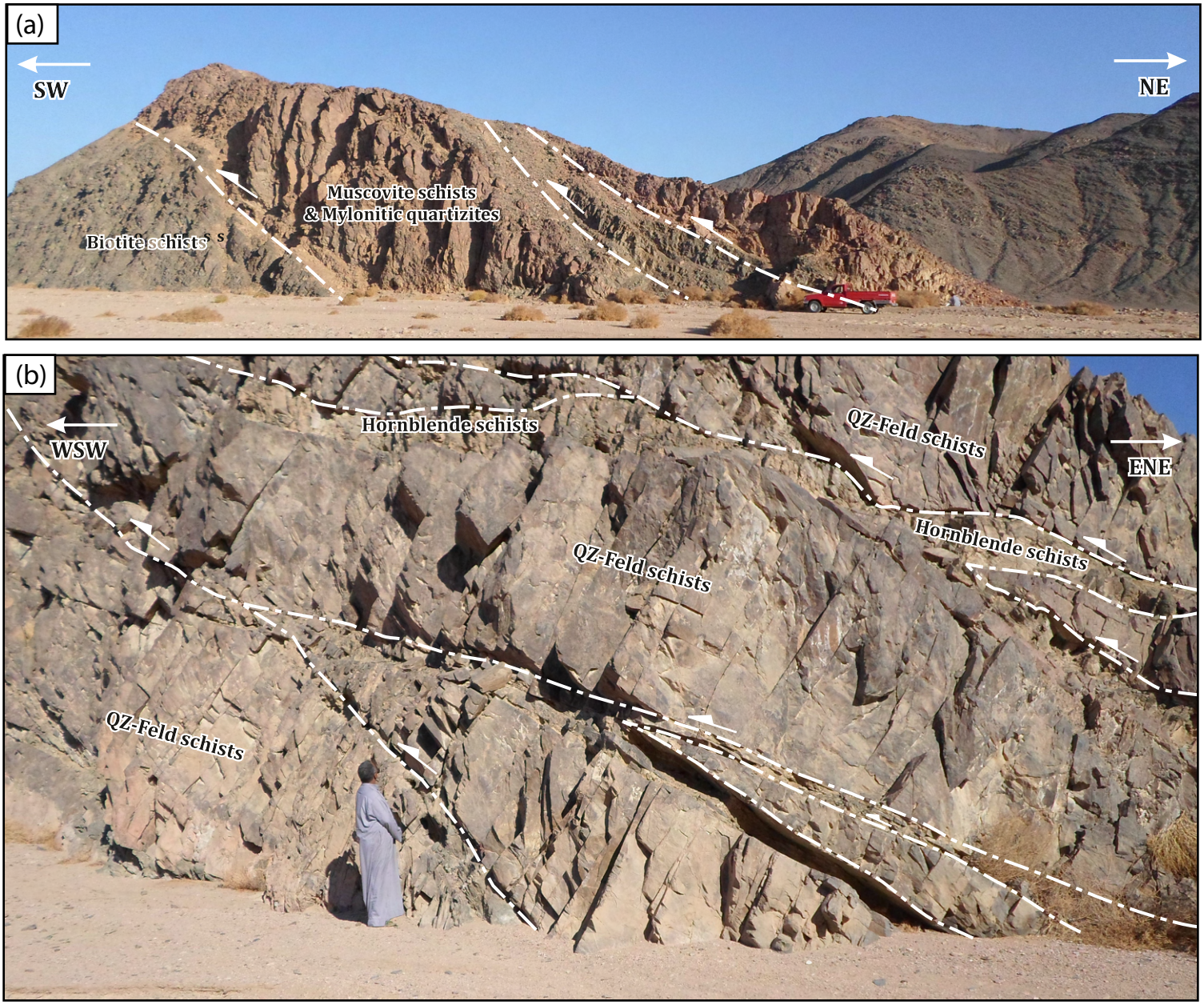
(a)
SW
NE
Muscovite schists
& Mylonitic quartizites
Biotite schists
(b)
WSW
ENE
Hornblende schists
QZ-Feld schists
QZ-Feld schists
Hornblende schists
QZ-Feld schists
(c)
NE
(d)
Normal faults
Thrust faults
(e)
NE
Normal faults
SW
Thrust faults
Fault plane

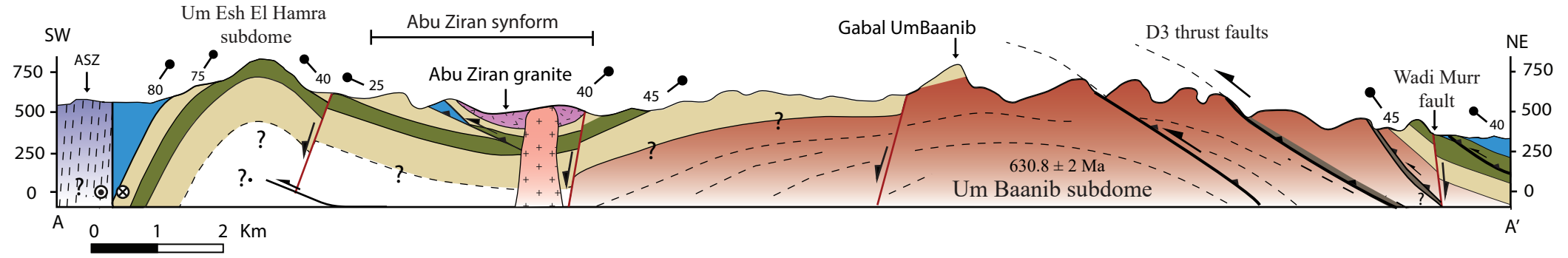

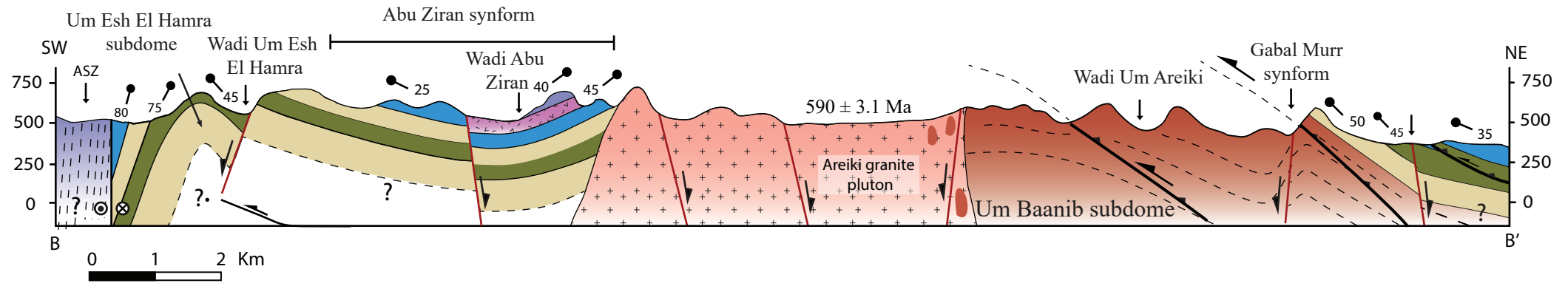

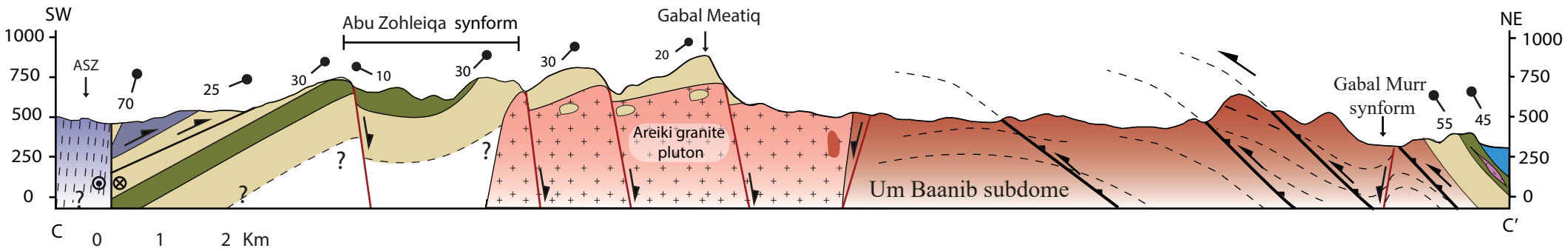

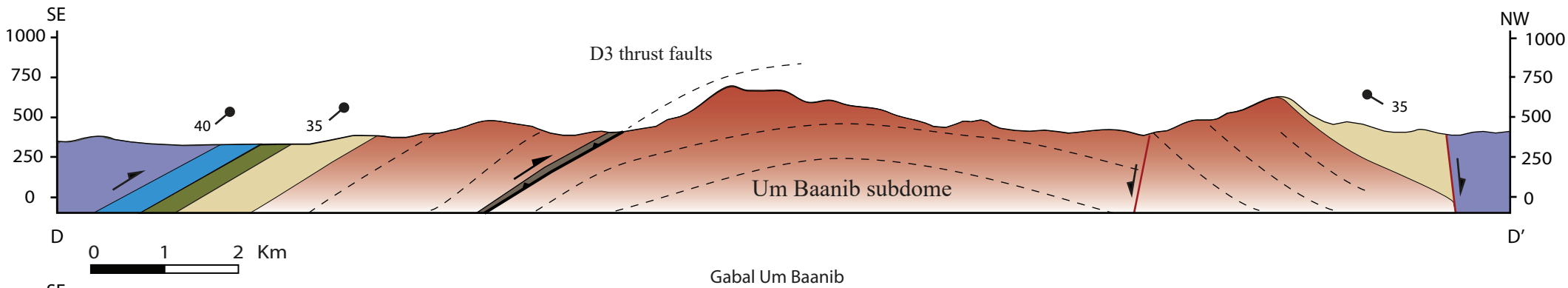

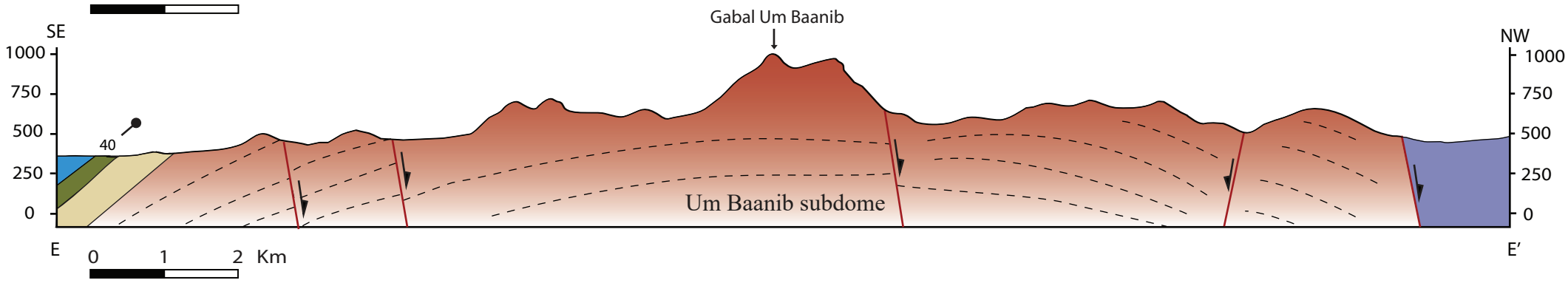

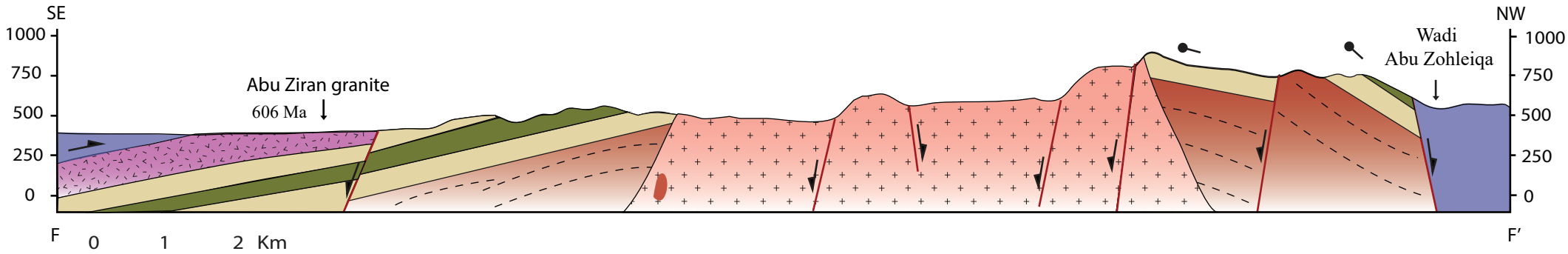

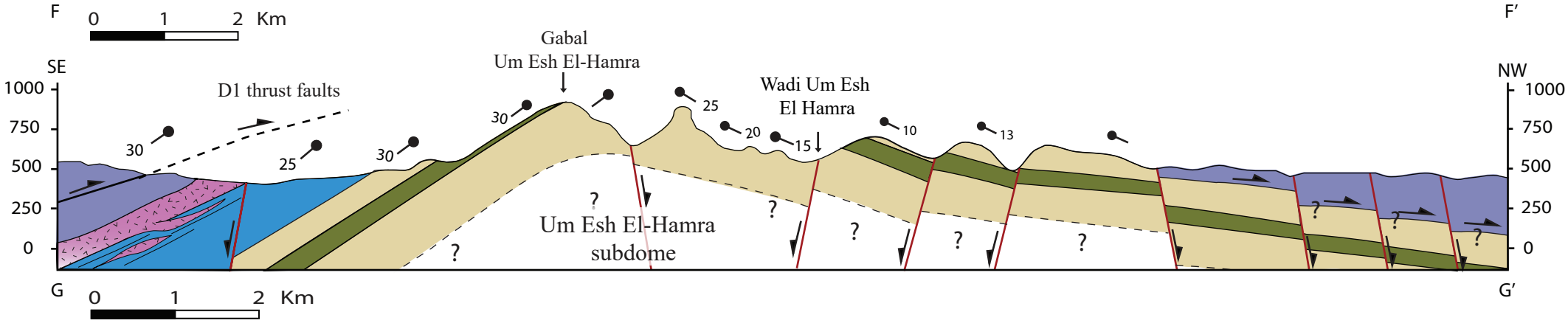

Legend

Tectonostratigraphic units

- Atalla Succession
- Meatiq Succession
  - Biotite- hornblende schist
  - Garnet-muscovite schist & phyllonites
  - Quartzo-feldspathic schist & mylonites

Granite intrusions

- Areiki granite
- Abu Ziran granite
- Um Baanib deformed granite

Structural symbols

- 10 — Dip andle and direction measured at surface
- Thrust shear zones with sense of movement
- Normal faults
- Thrust faults
- sinistral sense of shear along strike-slip shear zone

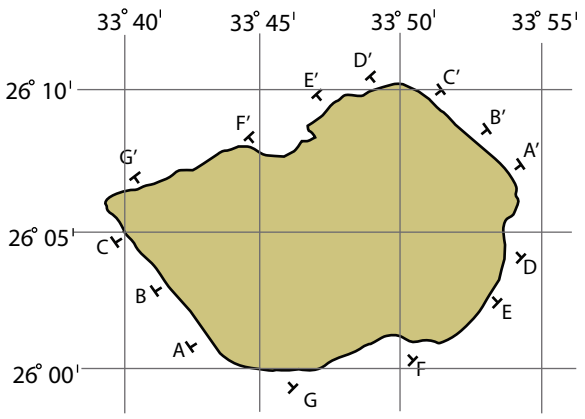

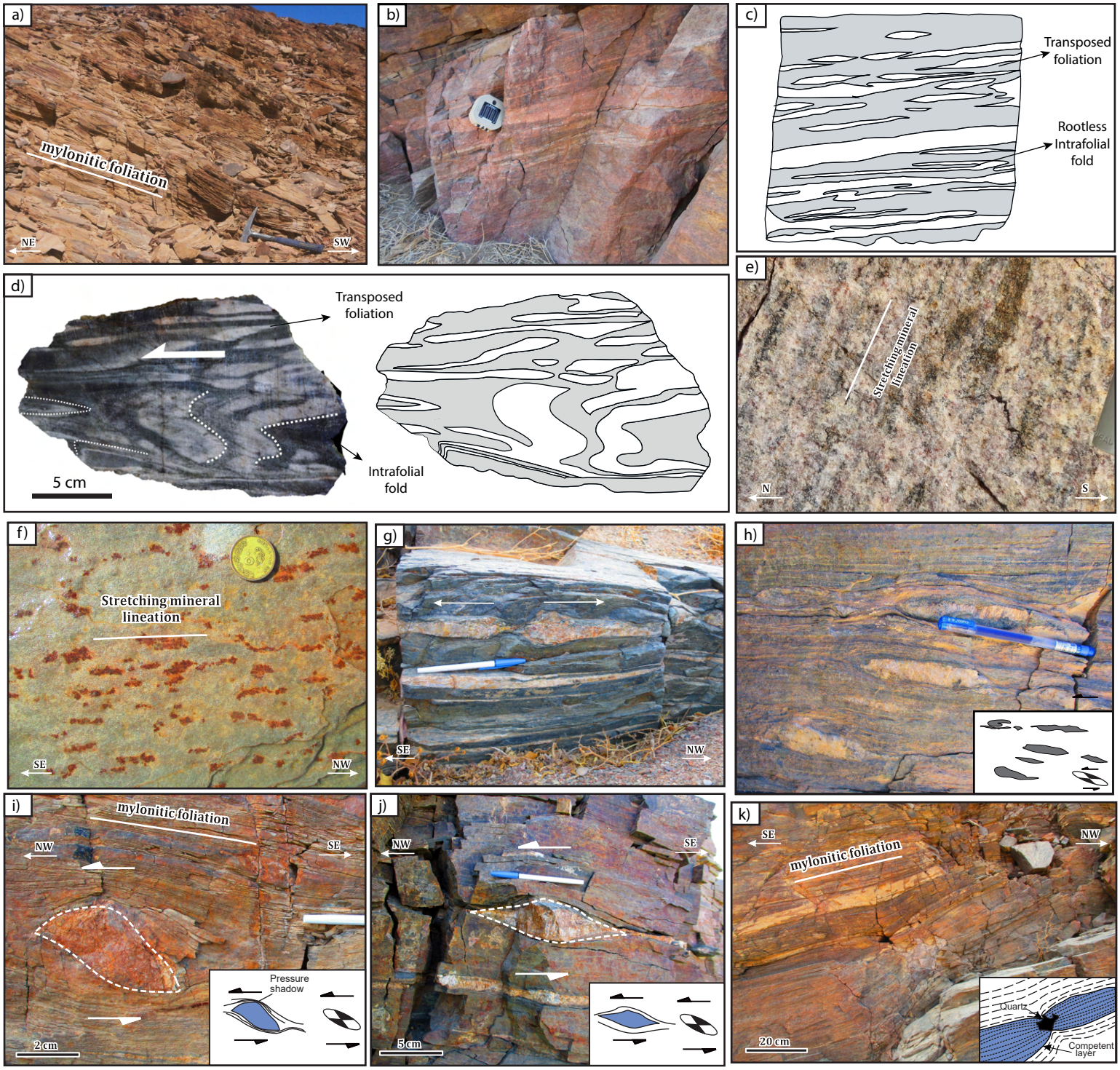
a)
mylonitic foliation
NE
SW
b)
c)
Transposed foliation
Rootless Intrafolial fold
d)
Transposed foliation
Intrafolial fold
5 cm
e)
Stretching mineral lineation
N
S
f)
Stretching mineral lineation
SE
NW
g)
SE
NW
h)
i)
mylonitic foliation
NW
SE
Pressure shadow
2 cm
j)
NW
SE
5 cm
k)
SE
NW
mylonitic foliation
20 cm
Quartz
Competent layer

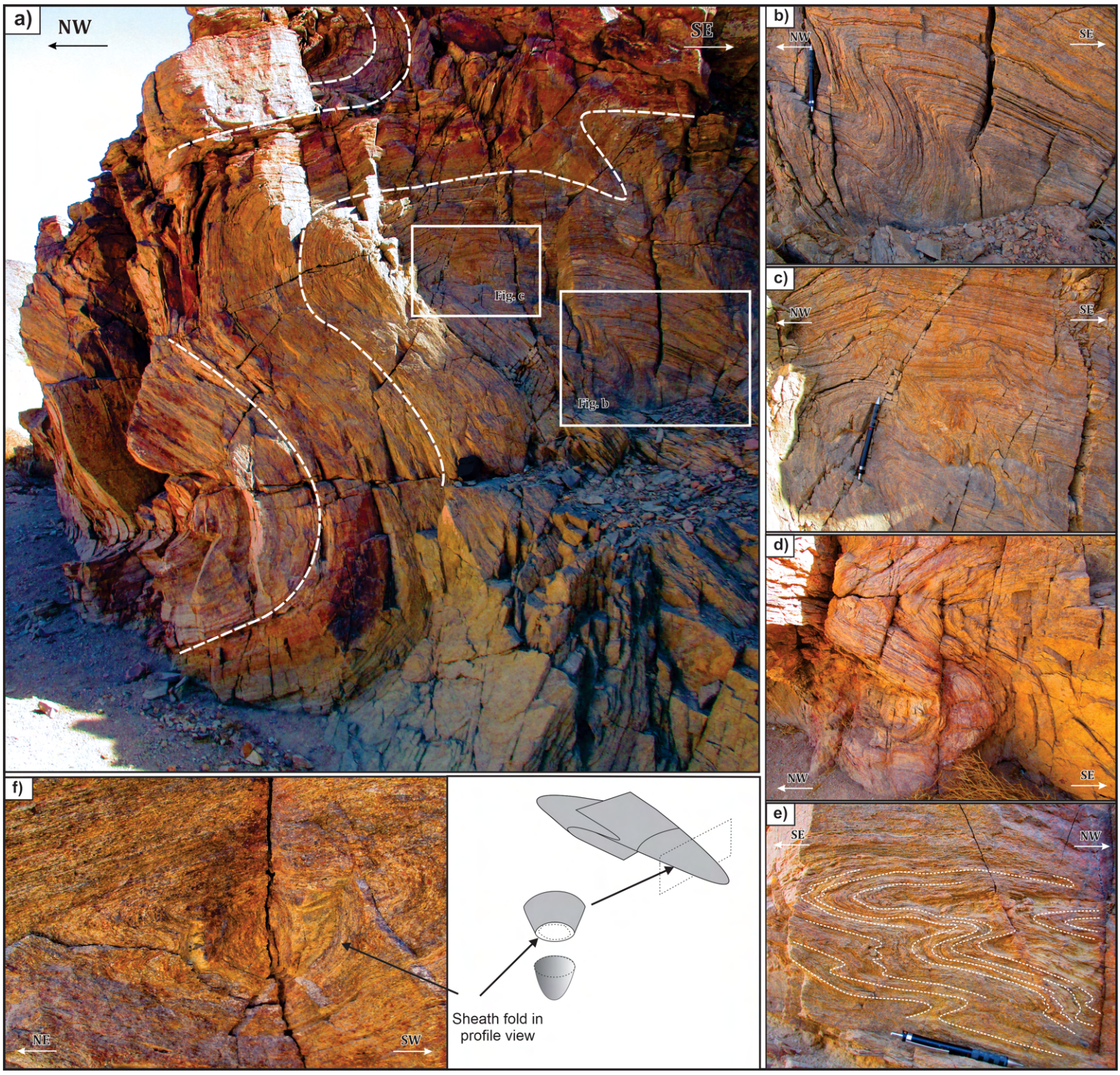
a)
NW
SE
Fig. c
Fig. b
b)
NW
SE
c)
NW
SE
d)
NW
SE
e)
SE
NW
f)
NE
SW
Sheath fold in
profile view

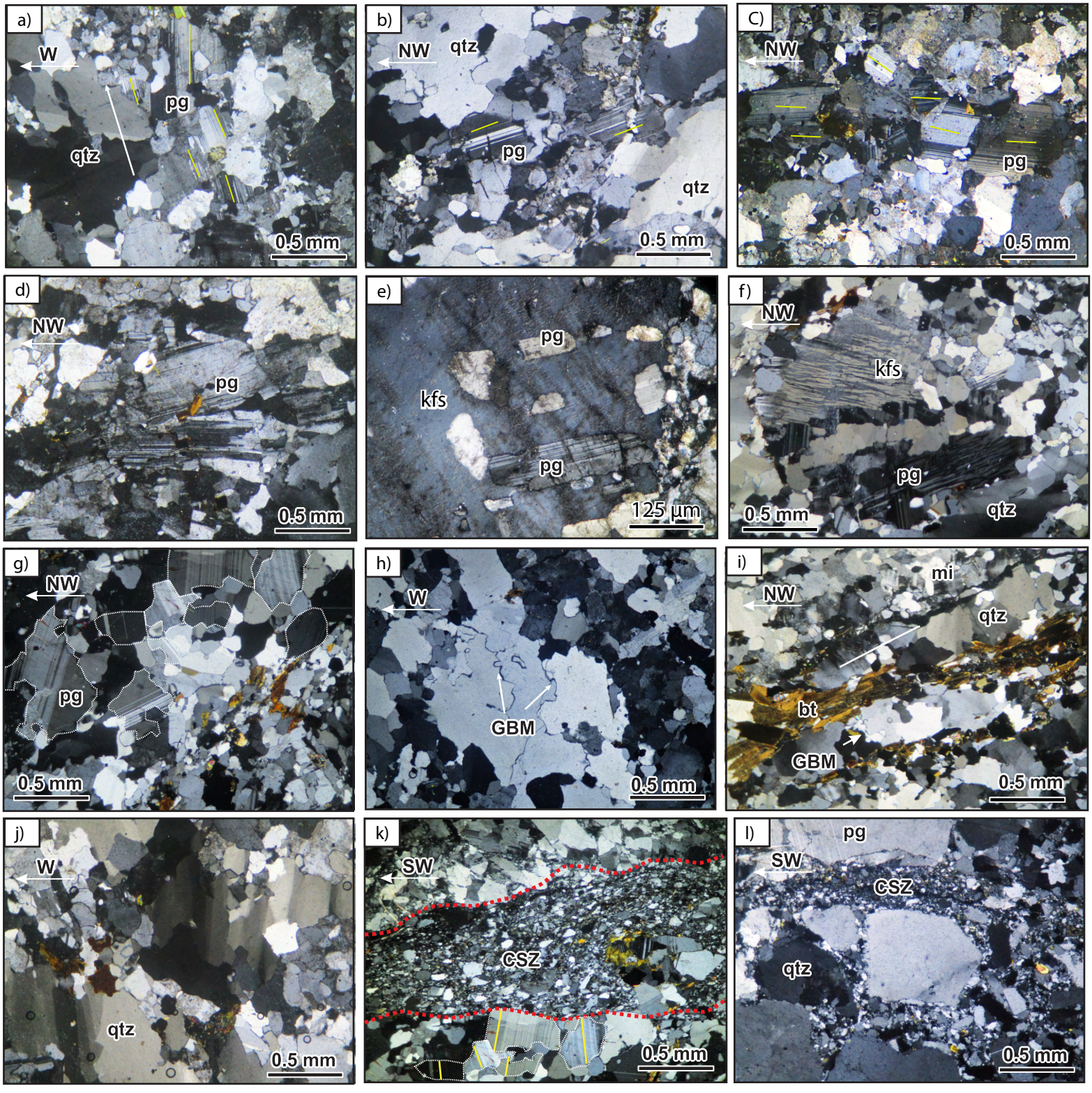
a)
W
pg
qtz
0.5 mm
b)
NW
qtz
pg
qtz
0.5 mm
C)
NW
pg
0.5 mm
d)
NW
pg
0.5 mm
e)
pg
kfs
pg
125 µm
f)
NW
kfs
pg
qtz
0.5 mm
g)
NW
pg
0.5 mm
h)
W
GBM
0.5 mm
i)
mi
NW
qtz
bt
GBM
0.5 mm
j)
W
qtz
0.5 mm
k)
SW
CSZ
0.5 mm
l)
pg
SW
CSZ
qtz
0.5 mm

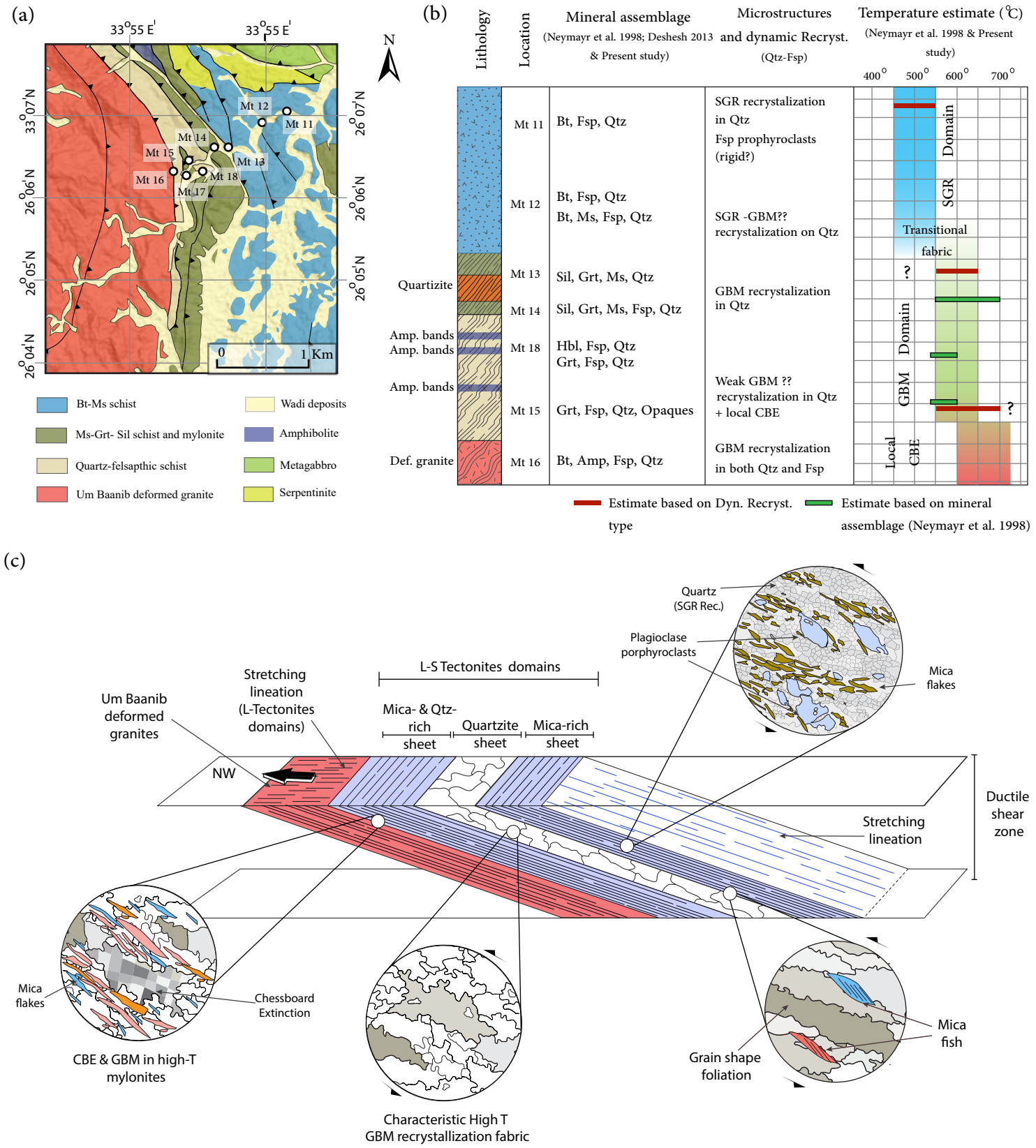
(a)
33°55 E'
33°55 E'
N
33°07'N
26°07'N
33°06'N
26°06'N
33°05'N
26°05'N
33°04'N
Mt 11
Mt 12
Mt 13
Mt 14
Mt 15
Mt 16
Mt 17
Mt 18
0
1 Km
Bt-Ms schist
Ms-Grt- Sil schist and mylonite
Quartz-felsapthic schist
Um Baanib deformed granite
Wadi deposits
Amphibolite
Metagabbro
Serpentinite
(b)
Lithology
Location
Mineral assemblage
(Neymayr et al. 1998; Deshesh 2013 & Present study)
Microstructures and dynamic Recryst.
(Qtz-Fsp)
Temperature estimate (°C)
(Neymayr et al. 1998 & Present study)
400°
500°
600°
700°
Quartizite
Amp. bands
Amp. bands
Amp. bands
Def. granite
Mt 11
Bt, Fsp, Qtz
SGR recrystalization in Qtz
Fsp prophyroclasts (rigid?)
Mt 12
Bt, Fsp, Qtz
Bt, Ms, Fsp, Qtz
SGR -GBM?? recrystalization on Qtz
Mt 13
Sil, Grt, Ms, Qtz
Mt 14
Sil, Grt, Ms, Fsp, Qtz
GBM recrystalization in Qtz
Mt 18
Hbl, Fsp, Qtz
Grt, Fsp, Qtz
Mt 15
Grt, Fsp, Qtz, Opaques
Weak GBM ?? recrystalization in Qtz + local CBE
Mt 16
Bt, Amp, Fsp, Qtz
GBM recrystalization in both Qtz and Fsp
Domain
SGR
Transitional fabric
Domain
GBM
Local
CBE
?
?
Estimate based on Dyn. Recryst. type
Estimate based on mineral assemblage (Neymayr et al. 1998)
(c)
Quartz (SGR Rec.)
Plagioclase porphyroclasts
Mica flakes
L-S Tectonites domains
Stretching lineation (L-Tectonites domains)
Um Baanib deformed granites
Mica- & Qtz-rich sheet
Quartzite sheet
Mica-rich sheet
NW
Ductile shear zone
Stretching lineation
Mica flakes
Chessboard Extinction
CBE & GBM in high-T mylonites
Characteristic High T GBM recrystallization fabric
Grain shape foliation
Mica fish

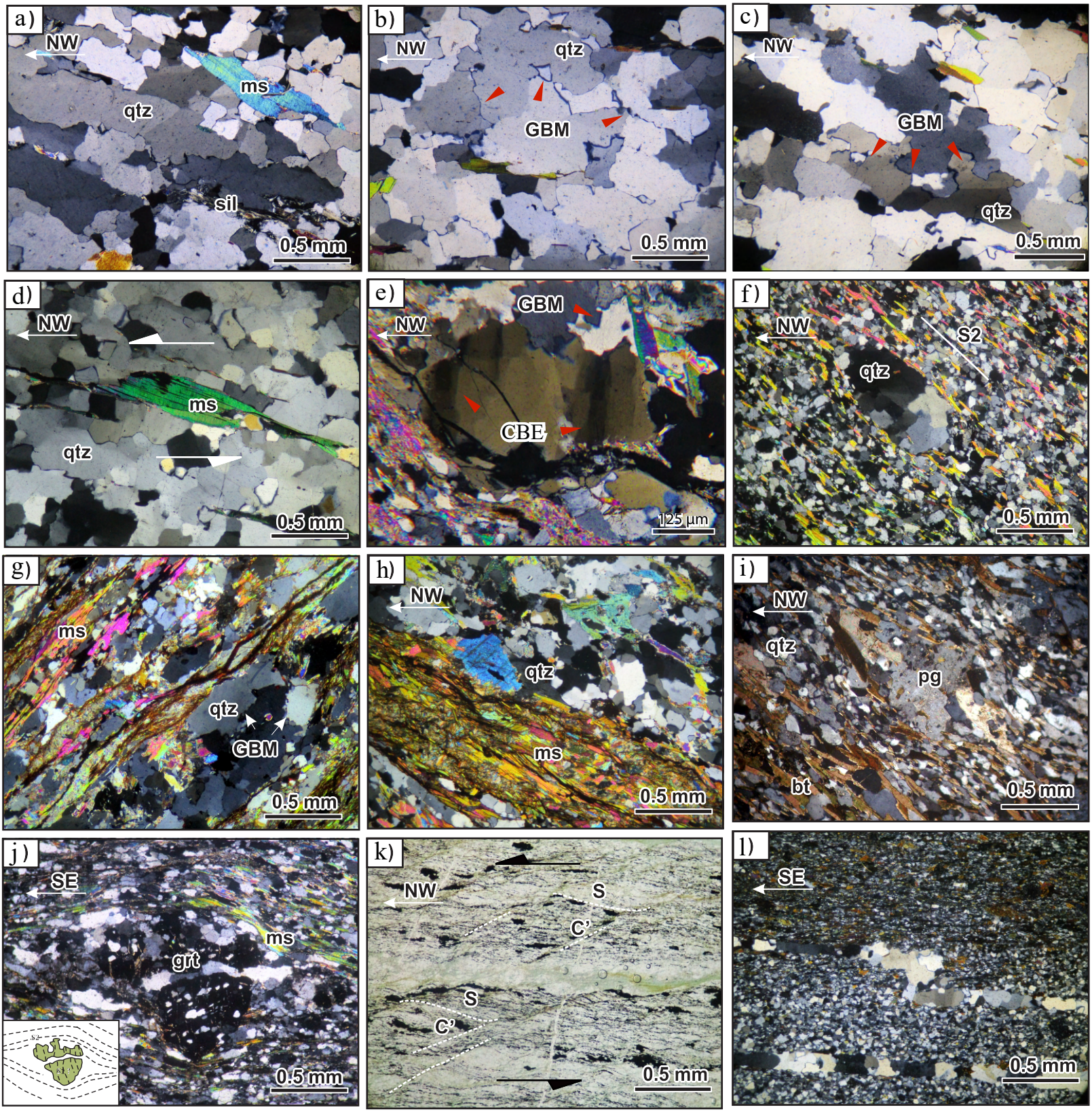
a)
NW
ms
qtz
sil
0.5 mm
b)
NW
qtz
GBM
0.5 mm
c)
NW
GBM
qtz
0.5 mm
d)
NW
ms
qtz
0.5 mm
e)
GBM
NW
CBE
125 µm
f)
NW
S2
qtz
0.5 mm
g)
ms
qtz
GBM
0.5 mm
h)
NW
qtz
ms
0.5 mm
i)
NW
qtz
pg
bt
0.5 mm
j)
SE
ms
grt
0.5 mm
k)
NW
S
C'
S
C'
0.5 mm
l)
SE
0.5 mm

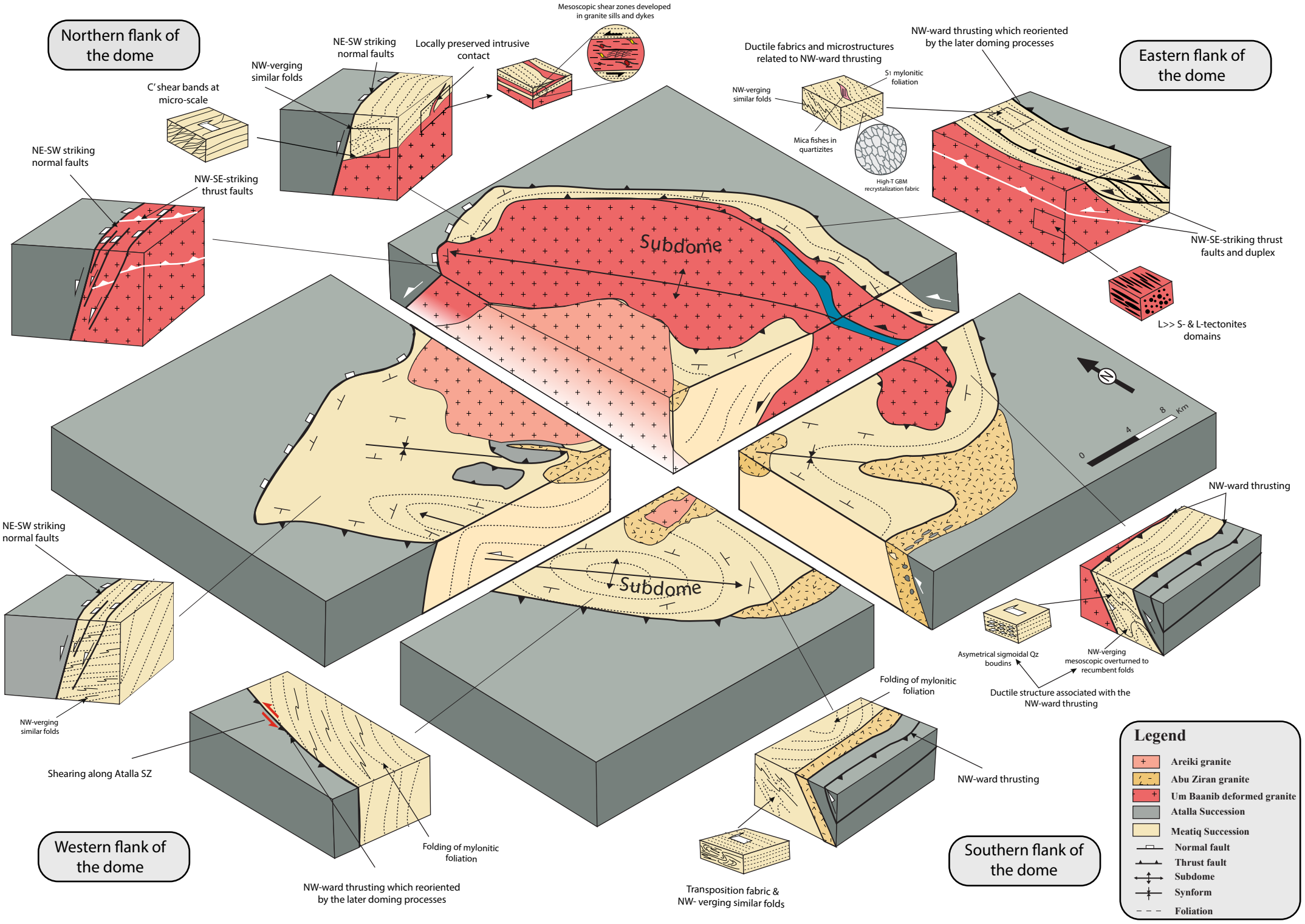
Northern flank of the dome
Mesoscopic shear zones developed in granite sills and dykes
Locally preserved intrusive contact
NE-SW striking normal faults
NW-verging similar folds
C' shear bands at micro-scale
NE-SW striking normal faults
NW-SE-striking thrust faults
Ductile fabrics and microstructures related to NW-ward thrusting
NW-ward thrusting which reoriented by the later doming processes
Eastern flank of the dome
S1 mylonitic foliation
NW-verging similar folds
Mica fishes in quartizites
High-T GBM recrystalization fabric
NW-SE-striking thrust faults and duplex
L>> S- & L-tectonites domains
Subdome
Subdome
N
0
4
8
km
NE-SW striking normal faults
NW-ward thrusting
NW-verging similar folds
Asymetrical sigmoidal Qz boudins
NW-verging mesoscopic overturned to recumbent folds
Ductile structure associated with the NW-ward thrusting
Folding of mylonitic foliation
Shearing along Atalla SZ
NW-ward thrusting
Folding of mylonitic foliation
Western flank of the dome
NW-ward thrusting which reoriented by the later doming processes
Transposition fabric & NW- verging similar folds
Southern flank of the dome
Legend
Areiki granite
Abu Ziran granite
Um Baanib deformed granite
Atalla Succession
Meatiq Succession
Normal fault
Thrust fault
Subdome
Synform
Foliation

a)

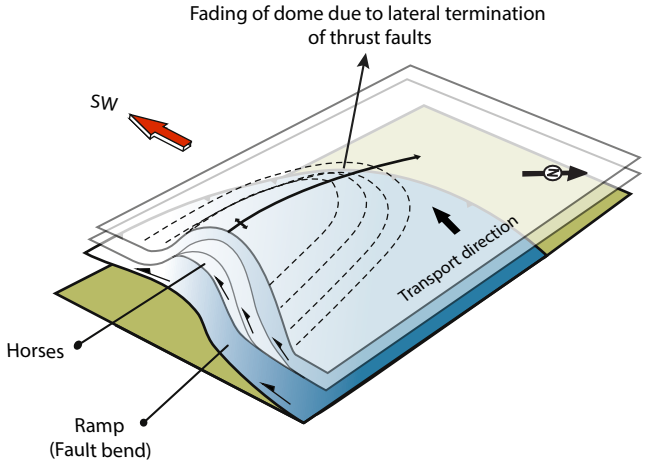

Antiformal stacking model

b)

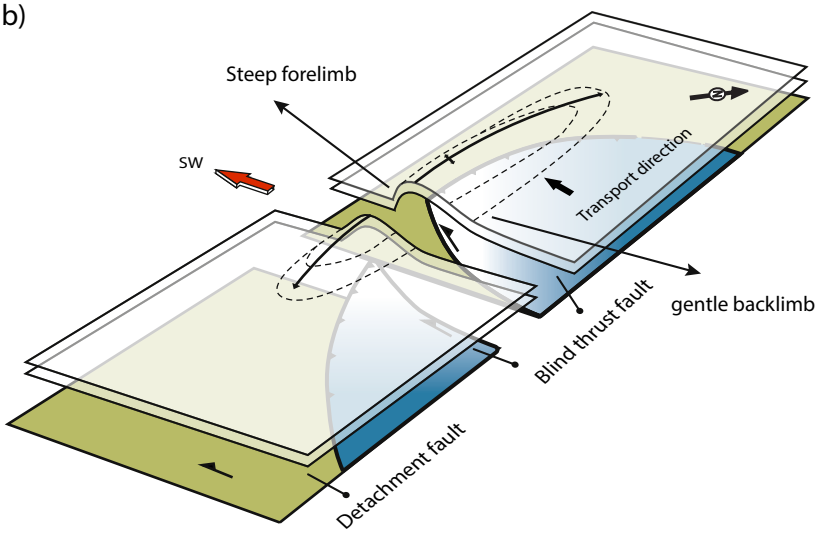

Fault propagation folding model

c)

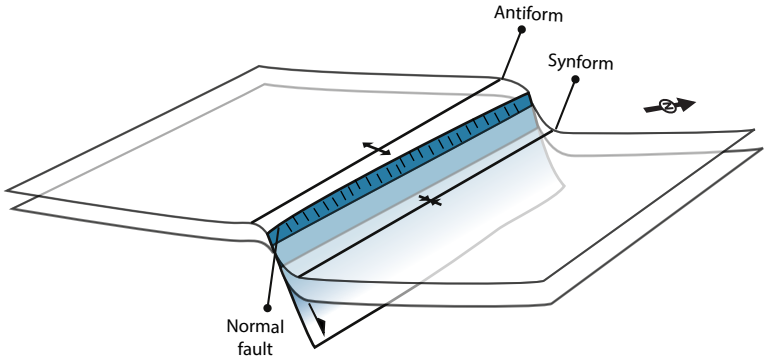

Extensional fault propagation folding model

a)

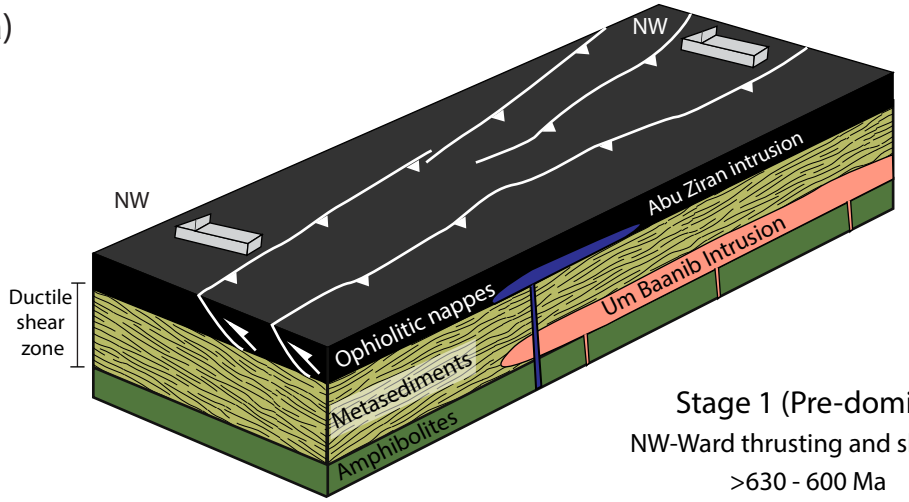

Stage 1 (Pre-doming)

NW-Ward thrusting and shearing

>630 - 600 Ma

b)

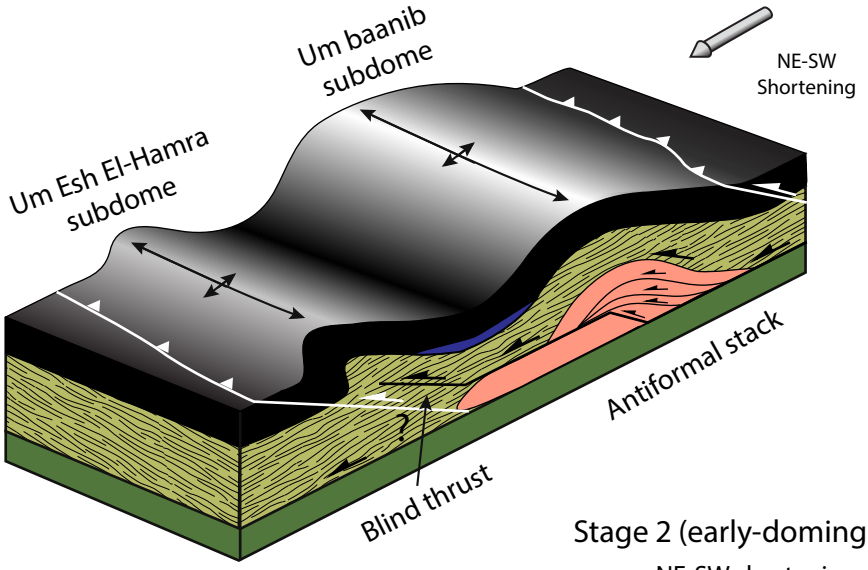

Stage 2 (early-doming stage)

NE-SW shortening

605-596 ??Ma

c)

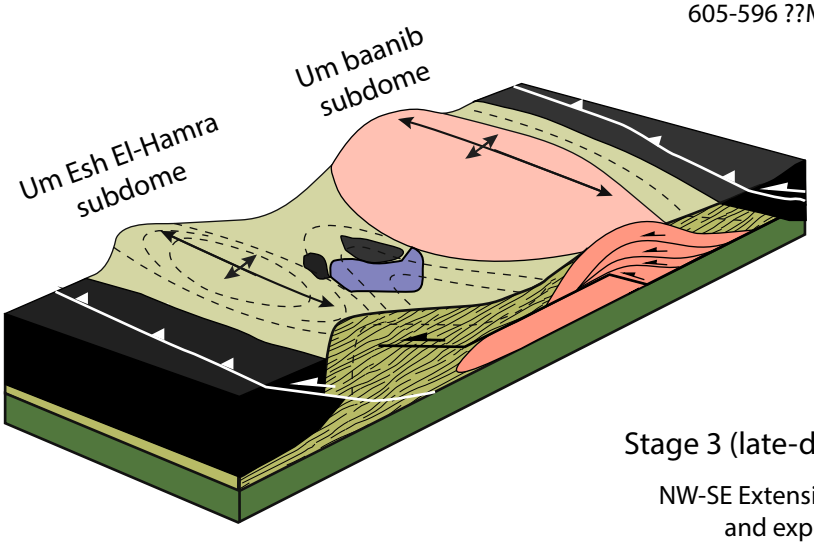

Stage 3 (late-doming stage)

NW-SE Extension, erosion and exposing

<590 Ma- Phanerozoic

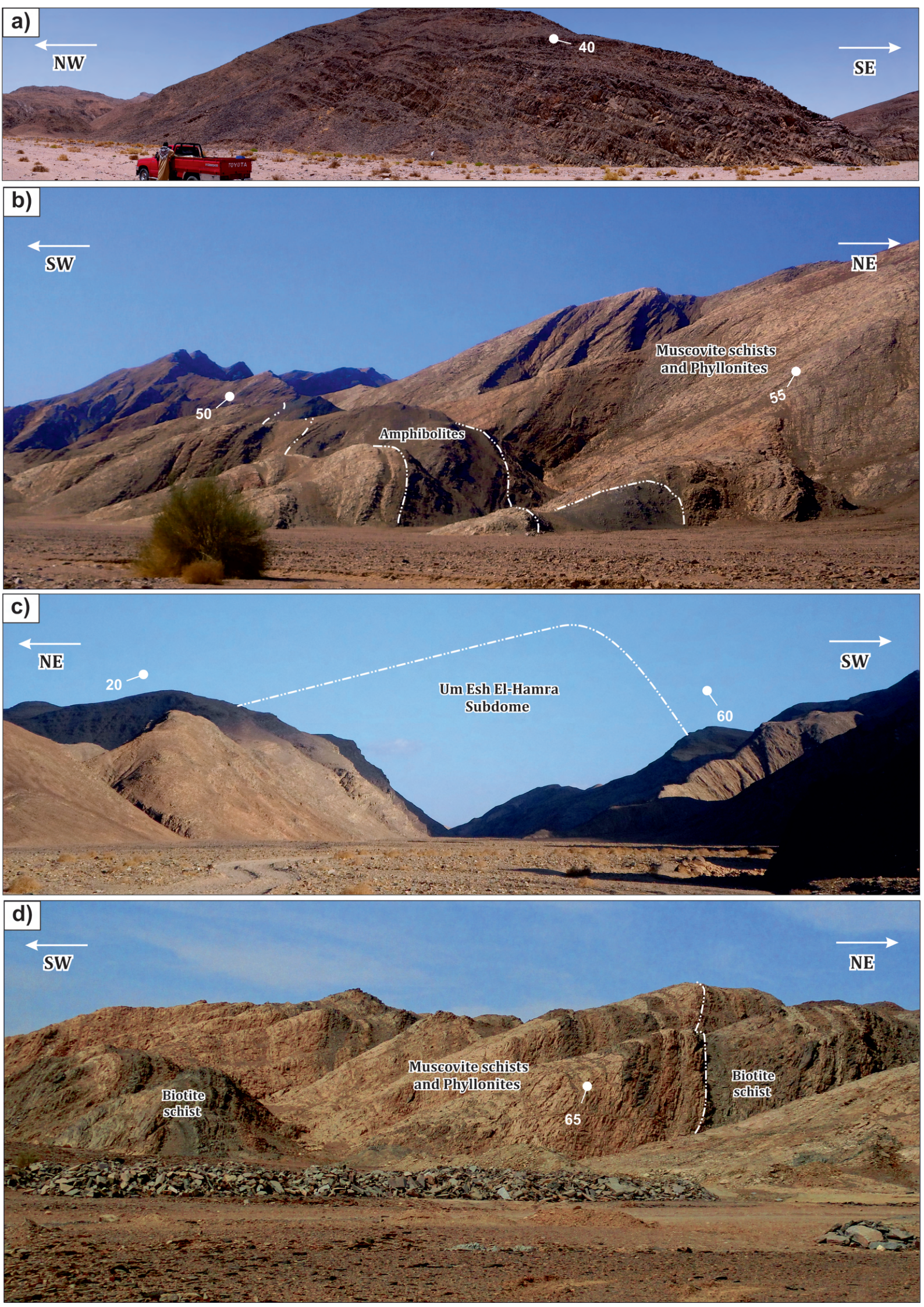
a)
NW
SE
40
b)
SW
NE
Muscovite schists
and Phyllonites
55
50
Amphibolites
c)
NE
SW
20
Um Esh El-Hamra
Subdome
60
d)
SW
NE
Biotite
schist
Muscovite schists
and Phyllonites
65
Biotite
schist

a)

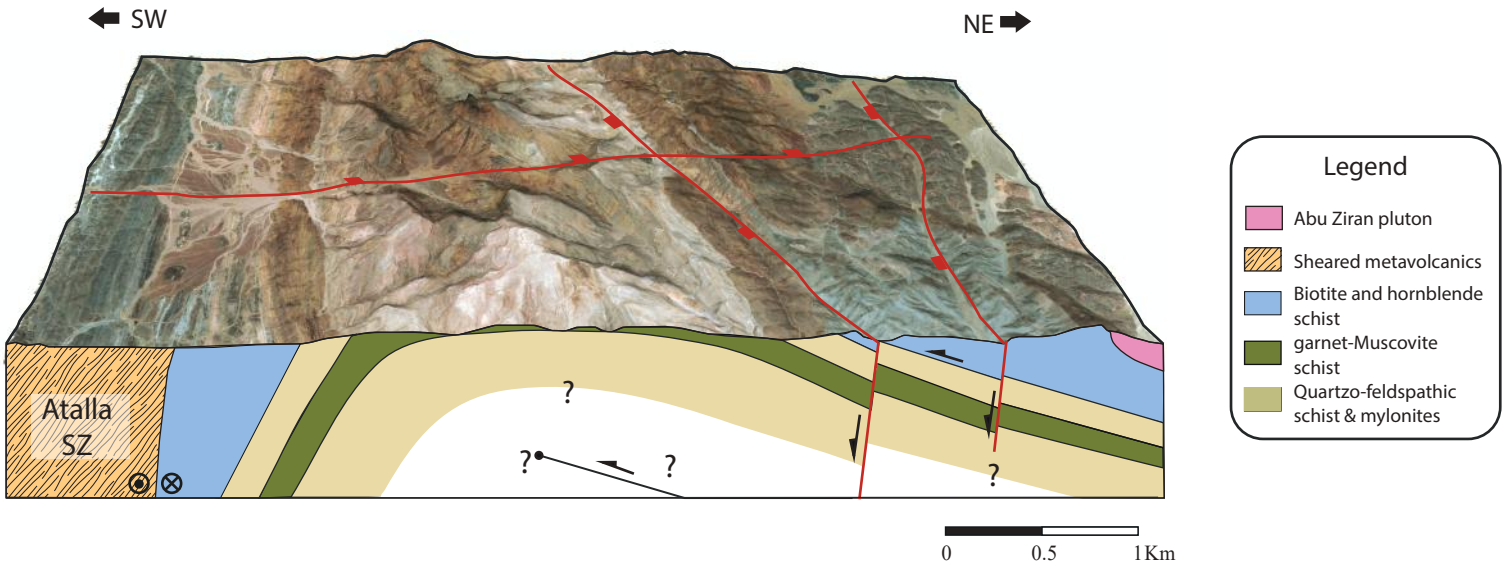
SW
NE
Atalla
SZ
?
?
?
?
0
0.5
1Km
Legend
Abu Ziran pluton
Sheared metavolcanics
Biotite and hornblende schist
garnet-Muscovite schist
Quartzo-feldspathic schist & mylonites

b)

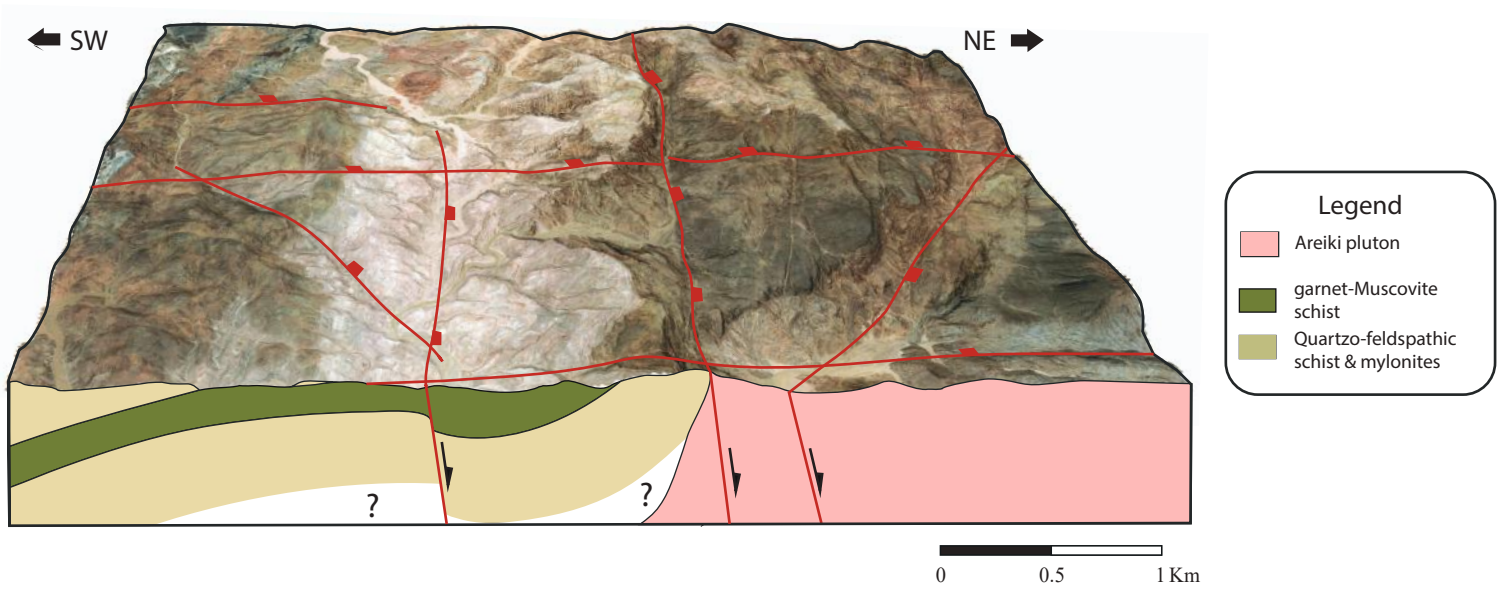
SW
NE
?
?
0
0.5
1 Km
Legend
Areiki pluton
garnet-Muscovite schist
Quartzo-feldspathic schist & mylonites

c)

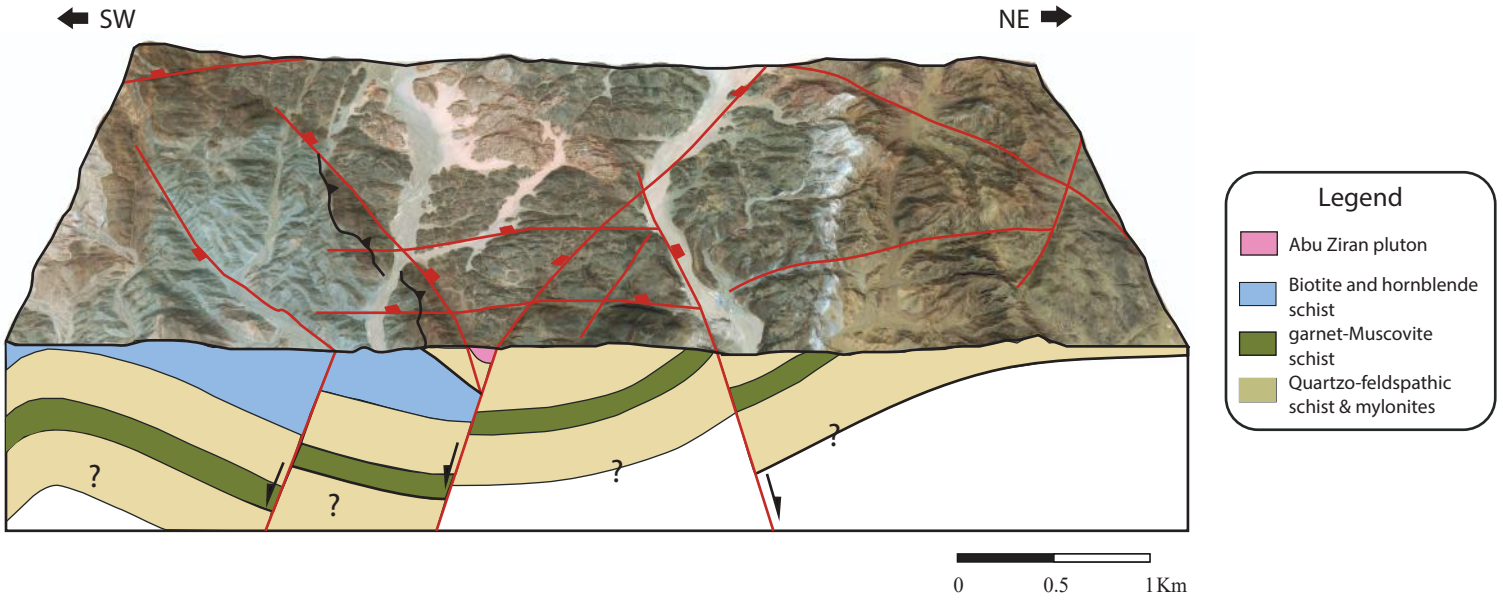
SW
NE
?
?
?
?
0
0.5
1 Km
Legend
Abu Ziran pluton
Biotite and hornblende schist
garnet-Muscovite schist
Quartzo-feldspathic schist & mylonites

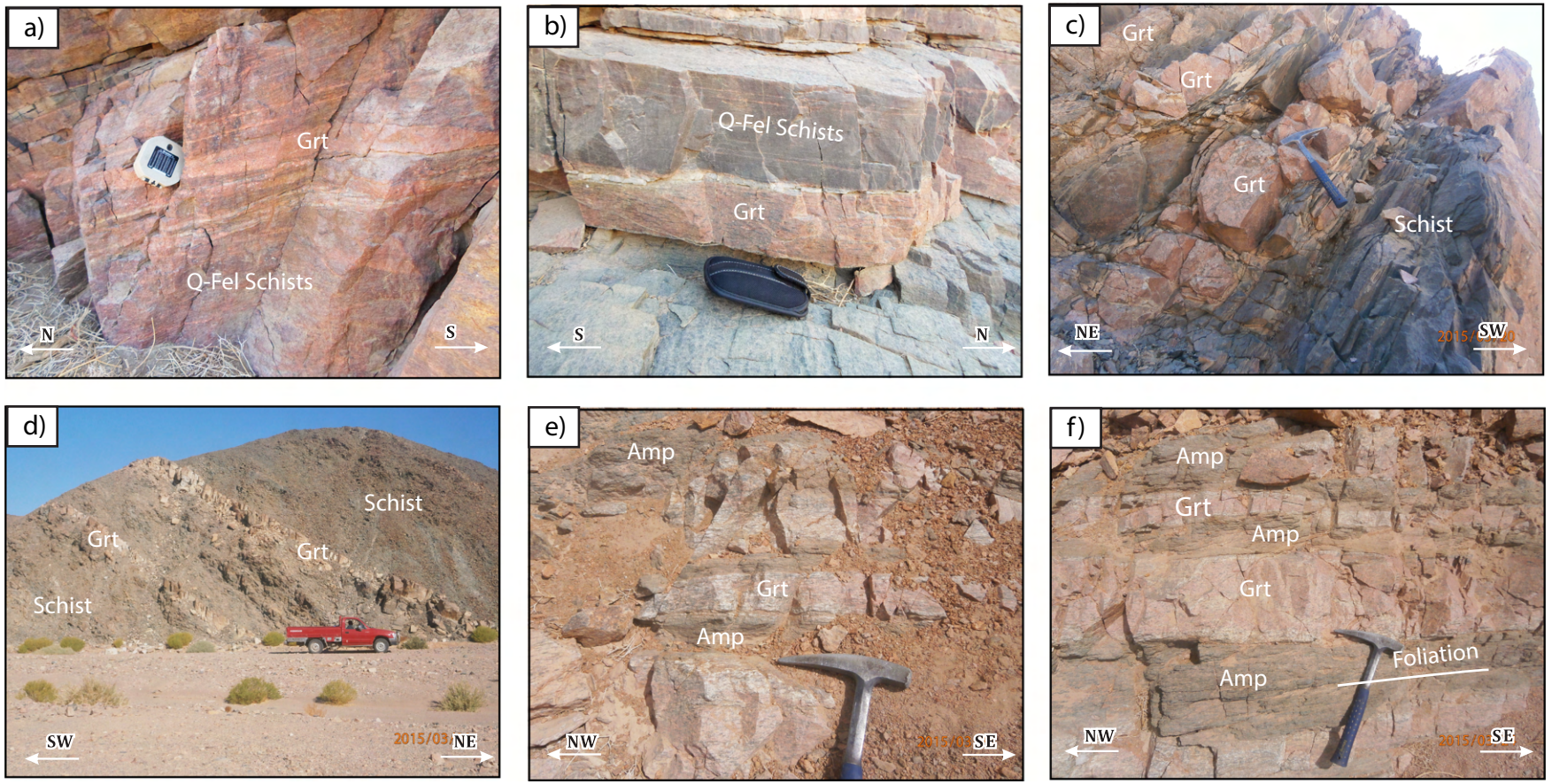

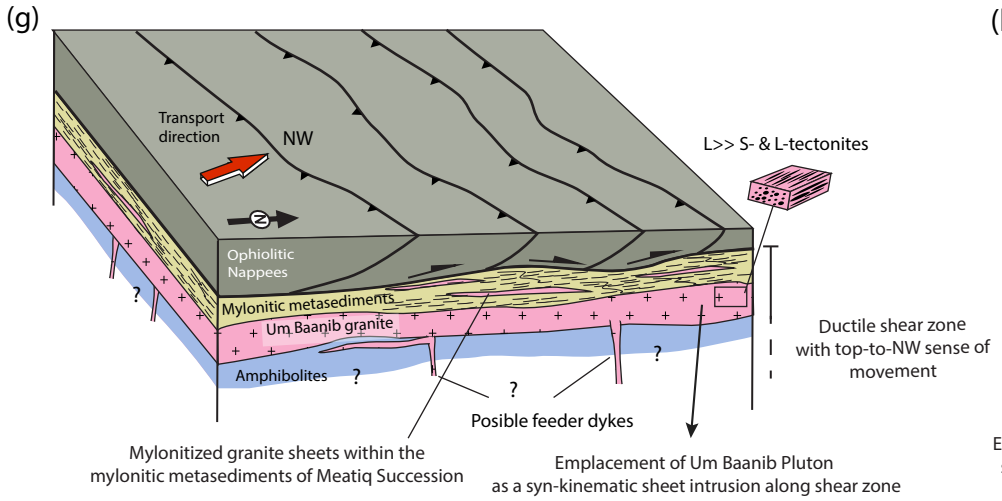

Emplacement of Um Baanib granite (630 Ma) earlier during the NW-ward thrusting

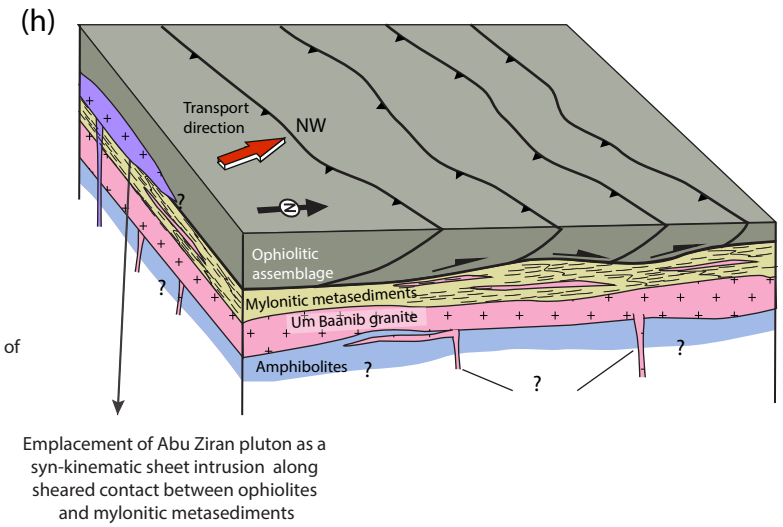

Emplacement of Abu Ziran granite (614-604 Ma) the final stages of NW-Ward thrusting and ceasing of deformation

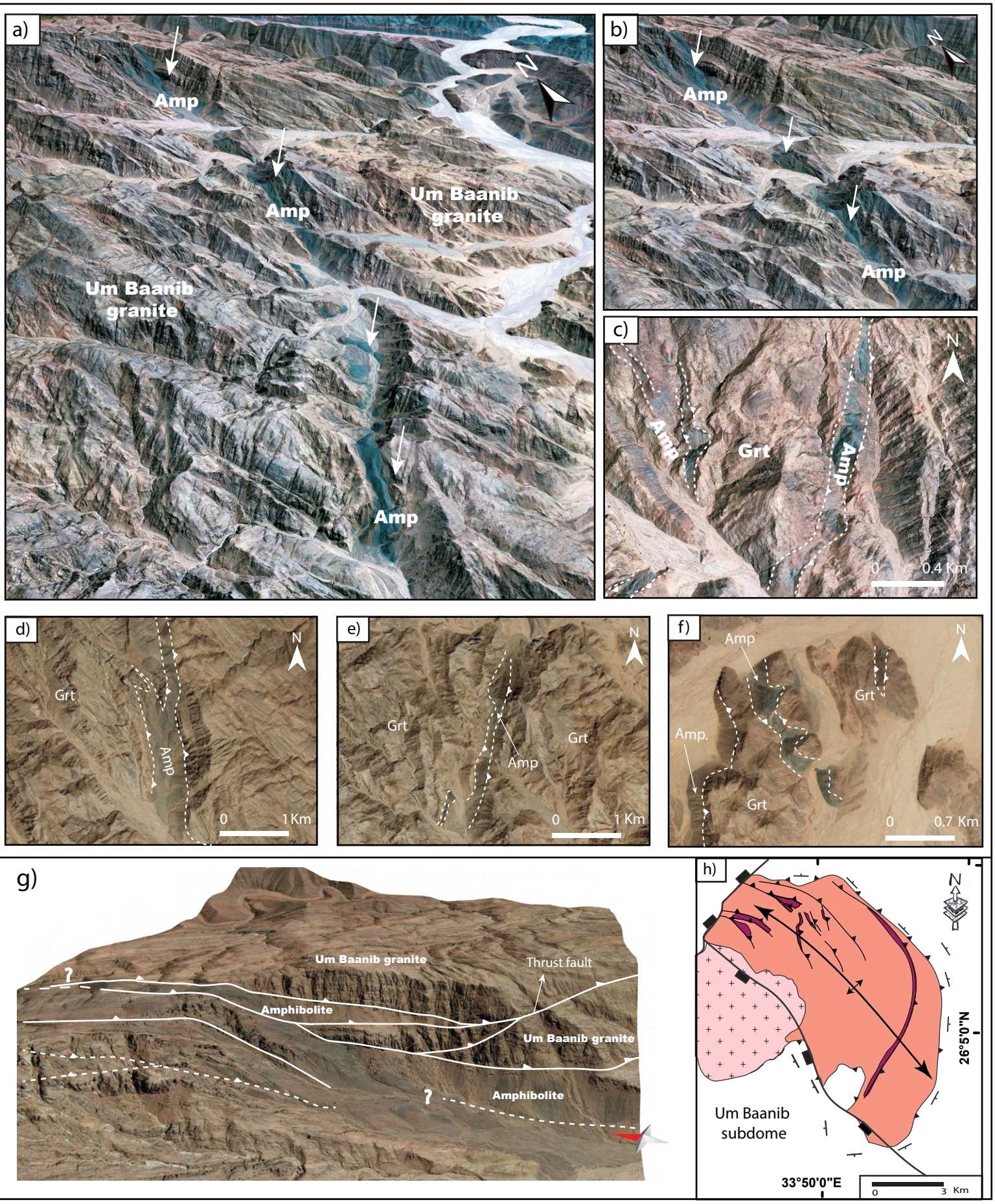
a)
Amp
Amp
Um Baanib granite
Um Baanib granite
Amp
N
b)
Amp
Amp
N
c)
Amp
Grt
Amp
N
0
0.4 Km
d)
Grt
Amp
N
0
1 Km
e)
Grt
Grt
Amp
N
0
1 Km
f)
Amp
Grt
Amp.
Grt
N
0
0.7 Km
g)
Um Baanib granite
Thrust fault
Amphibolite
Um Baanib granite
Amphibolite
?
?
h)
N
26°50'0"N
Um Baanib subdome
33°50'0"E
0
3 Km